Ordered-vacancy-compound semiconductors: Pseudocubic $CdIn_2Se_4$

James E. Bernard and Alex Zunger
Solar Energy Research Institute, Golden, Colorado 80401
(Received 21 September 1987)

Whereas *substitutional* adamantine compounds $A_nB_{4-n}C_4$ (e.g., ABC_2 chalcopyrites for $n=2$, or the AC and BC zinc-blende compounds for $n=4$ and 0) have four metal atoms around each nonmetal atom and vice versa, *ordered-vacancy compounds* (OVC's) AB_2C_4 have but three metal atoms (one A and two B's) around each nonmetal site (C) while the fourth (unoccupied) site forms an ordered array of vacancies. An example for OVC's is "pseudocubic" $CdIn_2Se_4$ which can be structurally derived from the layered alternate monolayer superlattice of CdSe and InSe (along the [001] direction) by removing half of the Cd atoms from each Cd plane. Such OVC's form a natural bridge between crystal and impurity physics. Much like the metal vacancy in II-VI compounds (e.g., CdSe), the vacancy in $CdIn_2Se_4$ has associated with it (nonmetal) "dangling bonds" and "lone-pair" electrons, which, however, form a dispersed band in the crystal. Using all-electron mixed-basis electronic-structure techniques, we study the properties of such an ordered array of vacancies in $CdIn_2Se_4$ *vis-à-vis* the experimental data. We find vacancy-induced atomic relaxations (Se moves towards the vacant site), resonant broadening of the lone-pair dangling-bond states into a $\approx$3-eV band, and that the total charge density around the vacant site has little density and shows scant evidence of dangling bonds. We discuss the nature of the bonding in this system, comparing it to other covalent selenides and to the observed photoemission and optical data. A number of possible order-disorder transitions, including the disordering of cations on the vacant sites, are identified.

I. INTRODUCTION

Ordered ternary adamantine semiconductors[1-13] $A_nB_{4-n}C_4$ ($n=1$, 2, and 3) are a natural structural extension of the well-known binary zinc-blende compounds AC and BC ($n=4$ and 0, respectively). They appear in 50%-50% combinations ($n=2$, or ABC_2) in either the layered tetragonal structure (Fig. 1(a), e.g.,[14] the CuAu I–like form such as $GaAlAs_2$, a structure analogous to an alternate monolayer superlattice of AC and BC grown along the [001] direction), or in the chalcopyrite structure (Fig. 1(d), e.g., $CuFeS_2$, analogous to the superlattice formed by depositing two layers of AC and two of BC along the [201] direction). For the 25%-75% ($n=1$) or 75%-25% ($n=3$) composition ratios they appear in either a Cu_3Au-like form [Fig. 1(b), e.g., lazarevicite, Cu_3AsS_4 (Ref. 15)] or the famatinite form [Fig. 1(c), e.g., Cu_3SbS_4 or $InGa_3As_4$ (Ref. 16)]. These four *substitutional* ternary structures have fourfold coordination (each cation surrounded by four anions and vice versa), near-tetrahedral angles, and satisfy the octet rule, like their parent zinc-blende structures (hexagonal, wurtzite-derived ternary structures exist too, but will not be discussed here).

There exists a class of ternary semiconductors analogous to substitutional $A_nB_{4-n}C_4$ where a given atomic site is *vacant in an ordered and stoichiometric fashion.* These AB_2C_4-type "ordered-vacancy compounds" (OVC's) can be structurally derived from their parent substitutional adamantine compounds by removing some of the atoms of type A. The "defect Cu_3Au" (or pseudocubic) structure of Fig. 1(e) can be derived from either the layered tetragonal CuAu I–like structure [Fig. 1(a)] or the Cu_3Au-like structure [Fig. 1(b)] by removing a cation from the base center of each layer. The "defect famatinite" (or "defect stannite," $H1c$) structure of Fig. 1(f) can be derived from famatinite [Fig. 1(c)] by removing alternately one base-centered and four corner cations of the famatinite structure; the "defect chalcopyrite" (or thiogallate, $E3$) structure [Fig. 1(g)] can be derived similarly from chalcopyrite [Fig. 1(d)]. As in substitutional adamantine compounds, in the OVC's [Figs. 1(e)–1(g)] each cation is coordinated by four nearest-neighbor anions. However, the anions are coordinated by two cations of one type, one of a different type, and one vacancy.

Ordered vacancy compounds (see reviews in Refs. 17 and 18) exhibit semiconducting properties, show a broad range of band gaps, form mutual solid solutions and manifest interesting optical and structural (e.g. order-disorder transitions) properties associated with the existence of a crystallographically ordered array of vacancies. They form a natural bridge between impurity physics (where, e.g., vacancies exist as isolated entities) and crystal physics (where each site is repeated translationally to form a sublattice). In this paper we study the electronic and structural properties of OVC's through first-principles electronic-structure calculations on the pseudocubic [Fig. 1(e)] $CdIn_2Se_4$ system, illustrating the analogies to both substitutional ternary compounds (e.g. $CuInSe_2$) and isolated vacancies in solids (e.g. the Cd vacancy in CdSe).

II. SIMPLE ELECTRONIC AND STRUCTURAL ANALOGIES TO $CdIn_2Se_4$

In this section we will review some simple expectations regarding the properties of OVC's, formulating the types

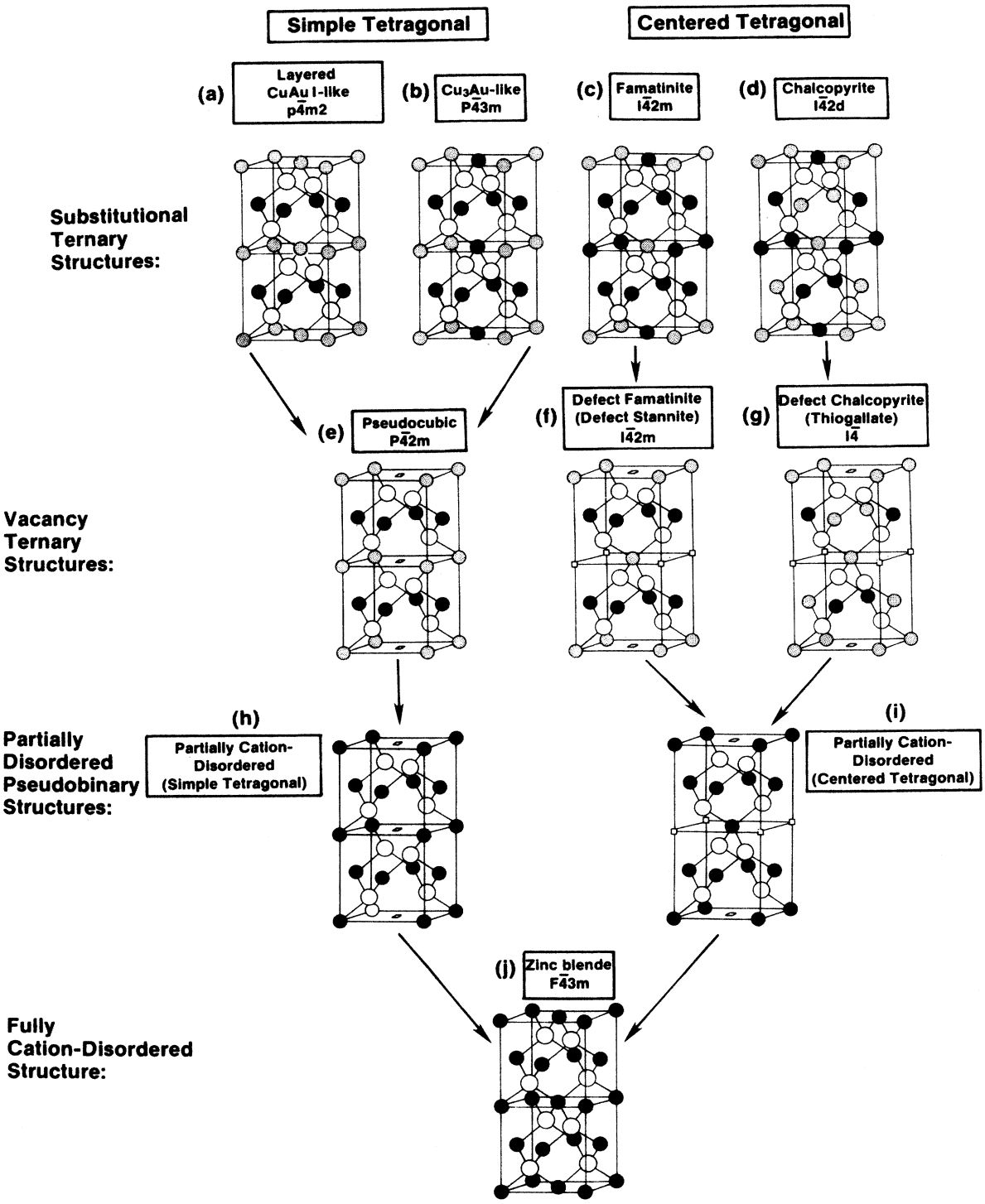

FIG. 1. Crystal structure of ternary $A_nB_{4-n}C_4$ adamantine compounds (a)–(d), vacancy structures derived from them (e)–(g), and two stages of cation disorder of the vacancy structures: Stage I, (h) and (i); and stage II, (j).

of questions to be addressed through electronic structure calculations on $CdIn_2Se_4$.

A. Lone-pair systems

Simple valence-bond arguments (Fig. 2) would suggest that in contrast to substitutional ternary compounds an OVC such as $CdIn_2Se_4$, would have lone-pair orbitals. Since In has three valence electrons (s^2p^1) and Cd has two (s^2), a fourfold-coordinated In would donate 3/4 electrons to each of its four In-Se bonds, while Cd will donate 2/4 electrons to each of its four Cd—Se bonds. Completing each bond to two electrons then requires that Se donate 5/4 electrons to the In—Se bond and 6/4

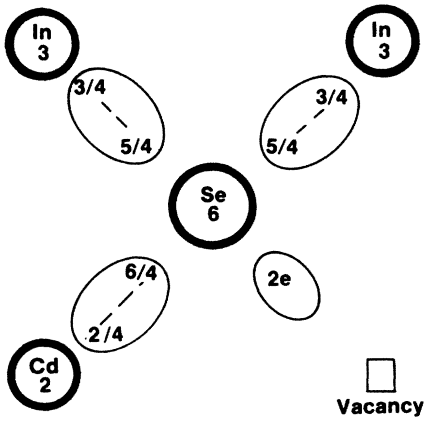

FIG. 2. A simple valence-bond model of bonding in $CdIn_2Se_4$, showing the possible existence of a lone pair orbital.

electrons to the Cd—Se bond. This leaves $6-2\times5/4-6/4=2$ out of the six Se electrons (s^2p^4) as a lone pair. The octet rule is satisfied as Se has two electrons in each of the four bonds around it. This simple valence-bond construct does not tell us if the lone-pair electrons are localized or delocalized in space, or whether they occur in a single orbital or in a band of states. One may wonder what might be the structural and electronic consequences of such a lone pair: in *molecular* species,[19] such lone pairs are often localized near a given atomic site, contributing thereby both to the chemical reactivity of this site and to the distortion of the bond lengths and angles relative to analogous compounds without a lone pair. This is the case in seleninyl fluoride[20] $SeOF_2$ (Se bonded to two F atoms and one oxygen, superficially analogous to $CdIn_2Se_4$ where Se is bonded to two In atoms and one Cd atom) where the two Se—F bonds (of length 1.73 Å) are slightly shorter than the ideal Pauling bond length (1.78 Å), whereas the Se—O bond (1.58 Å) is far shorter than the Pauling bond length (1.80 Å). We will identify the lone-pair states in $CdIn_2Se_4$ through self-consistent charge-density calculations and study their *distribution* both in *coordinate* space and in orbital *energy* space, establishing the degree of their localization (Sec. V E) and their effect on the optical properties (Sec. VI B).

B. Cation vacancy in II-VI compounds

The existence of an *undercoordinated* Se atom in $CdIn_2Se_4$ [Fig. 1(e)] suggests the cation vacancy in II-VI systems (e.g., Cd vacancy in CdSe or Zn vacancy in ZnSe) studied extensively both experimentally[21] and theoretically[22] as a natural analog. Applying the simple valence-bond argument of Sec. II A to the Zn vacancy in ZnSe one predicts that each of the three divalent (s^2) Zn sites contributes 2/4 electrons to each of the four Zn—Se bonds, whereas the six-electron (s^2p^4) Se atom complements each bond to two electrons by donating 6/4 of its electrons to each of the four bonds. This leaves on average $6-3\times6/4=1.5$ lone-pair electrons per Se–vacancy bond (a deficit of 0.5 electrons per bond), or (counting all four bonds) a total deficit of $4\times0.5=2$ electrons per vacancy. Electronic-structure calculations[22] on the unrelaxed *neutral* Zn vacancy in ZnSe (denoted V_{Zn}^0) show that this deficit is accommodated in a t_2 (*pd*-like) orbital, occupied by four electrons (out of a maximum occupancy of six electrons). The configuration is then $a_1^2t_2^4$, where the lower-lying a_1 orbital (*s*-like) is fully occupied. Adding one extra electron to the neutral vacancy results then in the single acceptor state V_{Zn}^- ($a_1^2t_2^5$), whereas adding two electrons to V_{Zn}^0 results in the double acceptor state V_{Zn}^{2-} ($a_1^2t_2^6$). The latter is spin-paired (hence, invisible to electron paramagnetic resonance, or EPR), occurs in *n*-type ZnSe with Zn vacancies,[21] but can be photoionized to give V_{Zn}^- which is EPR-visible.[21] The OVC $CdIn_2Se_4$ is hence isoelectronic with V_{Zn}^{2-}, and like it, has a single undercoordinated Se site which, however, is periodically repeated.

Two aspects of the V_{Zn}^{2-} system are pertinent, by analogy, to $CdIn_2Se_4$.

(i) The t_2 and a_1 vacancy levels of V_{Zn}^{2-} ($a_1^2t_2^6$) are energetically separated and occur well *above* the valence-band maximum E_v (calculated[22] values: $E_v+0.39$ eV for a_1 and $E_v+1.09$ eV for t_2). One can imagine that as the concentration of these vacancies is increased (toward the 25% limit pertinent to OVC's), these localized and narrow vacancy states will delocalize and broaden into *bands*. This analogy has three implications. *First,* it suggests that one could attempt to analyze the highest occupied states in $CdIn_2Se_4$ as the descendents of the (broadened) vacancy states (see Secs. V A and V E). *Second,* the occurrence of *smaller* band gaps E_g in an OVC ($E_g=1.5$ eV in $CdIn_2Se_4$), relative to its binary analogs ($E_g=1.85$ eV in CdSe, $E_g=1.2$ eV in InSe at low temperature) could be naturally thought of as a consequence of the occurrence of broadened "vacancy states" *above* the "natural" band edge. *Third,* if the broadening of a_1 and t_2 does not suffice to bridge the energy separation between them (or that between a_1 and E_v), one expects to find a region of low density of states (an "internal" gap) below the highest occupied state of $CdIn_2Se_4$. Indeed, Baldereschi *et al.*,[23] have reported such an internal gap in their earlier calculations. We examine this point in Secs. III C and VI B.

(ii) Virtually all calculations on cation vacancies in zinc-blende semiconductors (e.g., Ref. 22) show that the t_2 vacancy orbital is a *p*-type, vacancy-oriented dangling bond associated primarily with the *anion* orbitals, and localized mostly on the first nearest neighbors to the vacancy. The existence of such dangling bonds often leads to atomic relaxation of the anion. This analogy hence suggests an examination of the electronic charge density of the few highest occupied states of $CdIn_2Se_4$ in terms of such dangling orbitals and the possibility of atomic relaxation around the vacancy. This will be undertaken in Sec. VI E.

C. Analogies with binary compounds

Expectations based on the known electronic structures of the binary compounds zinc-blende CdSe (Ref. 24) and

layered InSe (Ref. 25) suggest the former to be more ionic and lack a covalent buildup of charge on the Cd—Se bond, whereas the latter (on account of the existence of occupied and bonding In p orbitals) shows a covalent charge buildup on the In—Se bond. The upper valence band in each of these compounds exhibits states associated with the respective (Cd—Se and In—Se) bonds. The *coexistence* of both Cd—Se and In—Se bonds in the same unit cell in $CdIn_2Se_4$ and the proximity of the In and Cd valence orbital energies [Cd, s at -7.20 eV; In s and p at -10.13 eV and -5.36 eV, respectively (Ref. 26)] then raises questions on the *relative distribution* of charge on these two bonds and possible charge transfer between them. One wonders, in particular, whether $CdIn_2Se_4$ exhibits distinct energy bands associated with the individual In—Se and Cd—Se bonds, or whether the states corresponding to those bonds are intermixed. This will be discussed in Sec. V A.

D. Summary of implications of analogies

The simple analogies described in this section suggest a number of questions to be addressed.

(i) Does an OVC have lone pairs? How are they distributed in coordinate space (on Se, Se–vacancy bond, etc.)? Are they confined to a narrow region of energy or spread through other bands?

(ii) Do OVC's have (a_1-like or t_2-like) dangling bonds analogous to those of cation-vacancies in II-VI's? Do they broaden in energy into *continuous* bands, or leave an internal gap? Are they vacancy oriented? Is their charge density localized preferentially on the vacant site or its nearest anions?

(iii) Is the local structure around the vacancy distorted relative to the ideal zinc-blende arrangement? Is the *length* of the Cd—Se and In—Se bonds characteristic of those in zinc-blende and substitutional ternary compounds (e.g., CdSe, $CuInSe_2$) or are they distorted?

(iv) Are there distinct energy ranges in the band structure exhibiting such pure In—Se and Cd—Se bonds, or are they intermixed? What is the relative charge distribution on these bonds?

III. STRUCTURE OF THE PSEUDOCUBIC PHASE

A. Structural phase transitions

Given the existence of an array of vacant sites, it is not obvious that OVC's would exhibit crystallographic room-temperature ordering, since the structure offers a number of possibilities for order-disorder phase transitions. Even assuming, as is the case in binary compounds, that anion-cation antisite defects (anion on cation site and vice versa) do not reach stoichiometric proportions, one can consider two levels of disorder in the system. The first we call "stage-I disorder," in which the two cations A and B in AB_2C_4 mutually substitute for one another. This leads in both the defect famatinite [Fig. 1(f)] and the defect chalcopyrite [Fig. 1(g)] OVC's to the same partially cation-disordered phase [Fig. 1(i)], whereas the pseudocubic structure [Fig. 1(e)] results after stage-I disorder in the distinct structure shown in Fig. 1(h). The fact that both defect famatinite and defect chalcopyrite disorder into the *same* structure is likely to be the reason why it was generally impossible[27] to determine unequivocally whether $ZnGa_2S_4$, $ZnGa_2Se_4$, $ZnGa_2Te_4$, $ZnAl_2Te_4$, $CdAl_2Te_4$, $HgAl_2Te_4$, and $HgGa_2Te_4$ are ordered in the defect famatinite [Fig. 1(f)] or in the defect chalcopyrite [Fig. 1(g)] phase. In "stage II disorder," one can further imagine that both of the two cation types *and* the vacancy disorder mutually. This results in the formation of the disordered zinc-blende-like phase [Fig. 1(j)] from either of the partially (cation) disordered phases shown in Figs. 1(h) and 1(i). The ten OVC's known to disorder[18] into this zinc-blende phase are $ZnAl_2Se_4$, $ZnAl_2Te_4$, $ZnGa_2S_4$, $ZnGa_2Se_4$, $ZnGa_2Te_4$, $ZnIn_2Te_4$, $CdAl_2Te_4$, $CdGa_2Se_4$, $HgAl_2Te_4$, and $HgGa_2Te_4$. Direct order-disorder transformations into this zinc-blende phase were observed by Mocharnyuk *et al.*[28] for $(CdGa_2Se_4)_x(CdIn_2Se_4)_{1-x}$ alloys [for $CdGa_2Se_4$, $T_c = 820\,^\circ$C]. If the transition temperature T_c is lower than the crystal growth temperature, only the disordered phase would be observed. This is the case for[18] Cu_2HgI_4 ($T_c \approx 69.5\,^\circ$C), Ag_2HgI_4 ($T_c \approx 50.5\,^\circ$C),[29] and $HgGa_2Te_4$,[27] all exhibiting only zinc-blende-type diffraction peaks. As the system disorders, a reduction in the band gap is observed, e.g., $E_g = 1.5$ eV for ordered $CdGa_2Te_4$ [$I\bar{4}$ structure of Fig. 1(g)], and $E_g = 1.4$ eV in its disordered zinc-blende phase [Fig. 1(i)]. Whereas order-disorder transformations were previously observed in ternary chalcopyrites $A^{\rm I}B^{\rm III}C_2^{\rm VI}$ and pnictides $A^{\rm II}B^{\rm IV}C_2^{\rm V}$ (see compilation of data in Ref. 30), where the difference in the valence of the disordering atoms A and B is *two*, one expects similar transitions to be even more prevalent (and occur at lower T_c's) in the ordered-vacancy $A^{\rm II}B_2^{\rm III}C_4^{\rm VI}$ compounds in which the A-B valence difference is but one, so that disordering is energetically less costly. This suggests that the material properties of OVC's (structural parameters, band gap, transport properties) may depend sensitively on growth temperature and on the growth and quenching *rates*, as these control the extent to which a (partial or complete) disorder or multiple-phase coexistence is "frozen into" the sample.

In addition to stage I and stage II disorder, one can imagine two further cation-vacancy disorder reactions in AB_2C_4, e.g., disordering of the A atom alone on the vacancy site, or disordering of the B atom on the vacancy site. No report exists on this type of disorder.

All of the disorder reactions discussed above could result in alteration of the nearest-neighbor environment of the anions, violating the octet rule locally, though not on average. For example, whereas the $CdIn_2$ neighbors of Se in the ordered form have a total of eight valence electrons, formation of Cd_2In and In_3 neighbors around two Se sites results locally in seven and nine electrons, respectively, although their average (eight) satisfies the octet rule. It is likely that such reactions, which violate the octet rule locally, involve considerably more energy cost than reactions which preserve the anion nearest-neighbor environment. However, such local violations of the octet rule were observed to occur in chalcopyrites, e.g., $ZnSnP_2$ disorders above T_c to give Zn_3Sn and $ZnSn_3$ local environments around the P site.[31] Even below T_c, anti-site de-

fects such as Cu_{In} or In_{Cu} have been identified in[32] $CuInSe_2$. It is possible, in principle, to build a structure with the correct stoichiometry and some disorder on the cation sublattice, while preserving the octet rule around each anion. For example, disordering of the Cd atoms and vacancies, subject to local preservation of the octet rule, is possible when all Cd atoms and vacancies in a given plane are interchanged, though there is no restriction on the status of other, parallel planes of Cd and vacancies. Similarly, restricted disordering of the In atoms and vacancies results in planes of cubes [of the type shown in Fig. 1(e)] which are completely ordered, but which may have adjacent planes of cubes with the c axis rotated by 90° about an axis orthogonal to the planes. Restricted disordering analogous to stage-I disorder is also possible, and generates a more disordered structure than the previous types, having no simple pattern. However, it, like truly random stage-I disorder, requires that some lattice sites be occupied by different atoms, hence raising the possibility of local relaxations of the cation lattice. For $CdIn_2Se_4$ these relaxations are likely to be quite small, since the atomic radii of Cd and In are quite similar.

We hence next examine the experimental evidence on the crystal structure of $CdIn_2Se_4$.

B. The observed crystal structure of $CdIn_2Se_4$

The first experimental determination of the structure of α-$CdIn_2Se_4$ [Fig. 1(e)] was performed by Hahn *et al.*[27] who determined the space group to be $P\bar{4}2m$ (D_{2d}^1). In addition to the lattice constants a and c (with ratio denoted $\eta=c/a$) there are two cell-internal structural parameters, consistent with the space-group symmetry, which describe displacements of the atomic positions from those of an unrelaxed (equal-bond-length, i.e., zinc-blende-like) structure. These are (i) x, denoting displacements of the Se atoms in the [110] and [1$\bar{1}$0] directions [Fig. 3(a)]; and (ii) z, denoting displacements of the Se atoms in the [001] and [00$\bar{1}$] directions [Fig. 3(b)].

The primitive lattice vectors of the unit cell are $(1,0,0)a$, $(0,1,0)a$, and $(0,0,\eta)a$, and the atomic positions within the unit cell, expressed in terms of (a,η) and (x,z), are

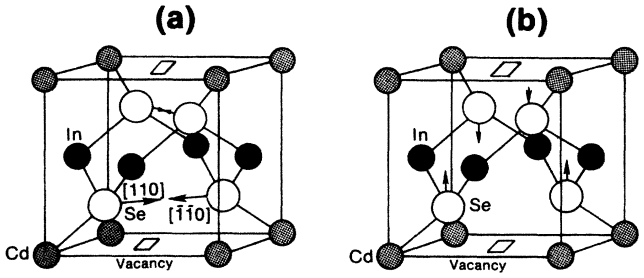

FIG. 3. Space-group preserving internal relaxations possible in the structure of pseudocubic $CdIn_2Se_4$. (a) shows the displacement of the anions as the parameter x is increased, and (b) shows the displacement as the parameter z is increased. See Eqs. (1) and (2). A square denotes the vacant site.

$$\begin{aligned}
&\text{Cd, } (0,0,0)a;\\
&\text{In, } (1/2,0,\eta/2)a;\\
&\text{In, } (0,1/2,\eta/2)a;\\
&\text{vacancy, } (1/2,1/2,0)a;\\
&\text{Se, } (x,x,z\eta)a;\\
&\text{Se, } (1-x,1-x,z\eta)a;\\
&\text{Se, } (x,1-x,(1-z)\eta)a;\\
&\text{Se, } (1-x,x,(1-z)\eta)a.
\end{aligned} \tag{1}$$

The three basic nearest-neighbor bond lengths (denoting the vacancy as V) obtained from Eq. (1) are

$$\begin{aligned}
R_{Cd-Se}(x,z,a,\eta)&=(2x^2+z^2\eta^2)^{1/2}a,\\
R_{In-Se}(x,z,a,\eta)&=[(x-1/2)^2+x^2+(z-1/2)^2\eta^2]^{1/2}a,\\
R_{V-Se}(x,z,a,\eta)&=[2(x-1/2)^2+z^2\eta^2]^{1/2}a.
\end{aligned} \tag{2}$$

The "unrelaxed structure" is defined as $x=z=1/4$ and $\eta=1$, which gives, in analogy with the zinc-blende structure, the equal-bond-length configuration

$$R_{Cd-Se}(1/4,1/4,a,1)=R_{In-Se}(1/4,1/4,a,1)=R_{V-Se}(1/4,1/4,a,1)=\frac{\sqrt{3}}{4}a. \tag{3}$$

The experimentally determined structural parameters are given in Table I.[27,33–35] The twenty-year-old *single-crystal* (Bridgman grown) work of Kawano and Ueda[35] ignored virtually by all recent (theoretical and experimental) work on this material, seems to be the most reliable one. Following earlier work by Suzuki and Mori[36] these authors have identified two structure types within their samples. The "fundamental" structure had the pseudocubic form [Fig. 1(e), parameters given in Table I], and, in addition, the "superstructure A" was identified in rotation photographs, in which a threefold increase in the cell parameter a of the pseudocubic structure was evident. This complex superstructure includes some Se tetrahedra with *two* vacancies.

Mixed phases in $CdIn_2Se_4$ have also been observed by others. Koval *et al.*,[37] using plate-shaped single crystals obtained by chemical vapor transport, have observed in addition to the pseudocubic structure also the defect chalcopyrite modification [Fig. 1(g)] with the same lattice parameters $a=c=5.815$ Å as observed later by Kawano and Ueda.[35] Przedmojski and Palosz[38] have obtained the same results for the lattice parameters and noted streaks

TABLE I. Experimentally observed structural parameters of α-$CdIn_2Se_4$.

Author and Sample	a (Å)	c/a	x	z	R_{Cd-Se} (Å)	R_{In-Se} (Å)
Hahn[a]	5.805	1.00	0.25	0.25	2.51	2.51
Kistaiah[b]	5.8207					
Trykozko[c]	5.823	1.00				
Kawano and Ueda[d]	5.815	1.00	0.2751±0.0001	0.2265±0.0001	2.61	2.62

[a]Reference 27: Synthesized by reacting binary compounds at 900 °C, followed by homogenization at 600 °C.
[b]Reference 33: Material grown by iodine chemical transport. Powder data collected at room temperature were obtained after annealing at 400 °C for 15 hours.
[c]Reference 34: Material grown by iodine vapor phase chemical transport, reacted at 670 °C and crystallized at 620 °C. Room temperature powder diffraction data are given.
[d]Reference 35: Single crystals grown by Bridgman method. Single-crystal x-ray data carefully refined, with observed refinement factor $R=0.077$.

in the diffraction pattern characteristic of the occurrence of stacking faults in the structure. Manolikas *et al.*,[39] have recently observed in high-resolution electron microscopy three polytypes of $CdIn_2Se_4$ with $\eta=c/a=1$, 2, and 4, where the first one is the pseudocubic structure, and the latter two are tetragonal polytypes, related to the former by antiphase domain boundaries.

It is obvious from these studies that even the best $CdIn_2Se_4$ crystals to date involve some structural disorder and are not single-phase materials. In what follows we will study the properties of the majority species (the pseudocubic phase) and proceed with caution when predicted results for this phase are compared with the experimental data on imperfect samples (Sec. VI).

C. Modeling the structural distortions in pseudocubic $CdIn_2Se_4$

To gain some insight into the structural parameters of pseudocubic $CdIn_2Se_4$ (Table I), we consider a simple semiclassical model. Following the "conservation of tetrahedral bonds" (CTB) model of Jaffe and Zunger,[40] we assume that to lowest order (i.e., neglecting finite bond-bending force constants), the structural parameters x,z,a,η of the pseudocubic phase would assume those values which make the bond lengths R_{Cd-Se} and R_{In-Se} equal to the *ideal tetrahedral bond lengths*, i.e.

$$R_{Cd-Se}(x,z,a,\eta)\equiv d^0_{Cd-Se}$$
$$R_{In-Se}(x,z,a,\eta)\equiv d^0_{In-Se}. \tag{4}$$

Here, d^0 can be taken to be Pauling's tetrahedral atomic radii[41] [$R(Cd)=1.48$ Å, $R(In)=1.44$ Å, and $R(Se)=1.14$ Å], yielding $d^0_{Cd-Se}=2.62$ Å, identical to the experimental value[42] in cubic CdSe, and $d^0_{In-Se}=2.58$ Å, close to the value of 2.59 Å observed[40,43] in $CuInSe_2$. This CTB model then assumes that bond-bending force constants in fourfold-coordinated adamantine compounds are sufficiently smaller than bond-stretching force constants that the equilibrium structure minimizes its strain energy by minimizing deformations such as $(R_{AC}-d^0_{AC})^2$ (at the expense of some distortions of the bond angles away from the ideal tetrahedral value, see Fig. 4 below). This approach predicted accurately the cell-internal distortion parameters in chalcopyrites and pnictides.[40,44] Inclusion of bond-bending elastic terms provides but a small correction.[45]

To solve Eqs. (2) and (4) we set $\eta=1$ and $a=5.815$ Å, both taken from the experimental data of Kawano and Ueda,[35] and find

$$x(\mathrm{CTB})=0.272,$$
$$z(\mathrm{CTB})=0.234 \tag{5a}$$

which are very close to the best experimental results[35]

$$x(\mathrm{expt})=0.2750,$$
$$z(\mathrm{expt})=0.2265. \tag{5b}$$

Figure 4 compares the local bond geometry of the CTB model with that actually observed in pseudocubic $CdIn_2Se_4$, revealing close agreement between the two. This shows that the observed distortions underlying the OVC structure merely manifest the tendency of covalent bonds to attain their ideal tetrahedral value. The distortion pattern shows that Se moves towards the vacancy by 0.10 Å and away from Cd and In by a similar amount. We refer to this structural model as the "fully relaxed" CTB model. Figure 5 shows contours of the Cd—Se bond length [Fig. 5(a)] and the In—Se bond length [Fig. 5(b)] as a function of the cell-internal parameters x and z for $a=5.82$ Å and $\eta=1$ [Eq. (2)]. The fully relaxed CTB structure is denoted there as the point marked CTB, the unrelaxed (UR) structure is denoted as UR, and the observed[35] structure is denoted as Expt.

Since the accurate experimental determination[35] of the structural parameters of $CdIn_2Se_4$ was overlooked by previous authors, various theoretical schemes were proposed to estimate x and z. Baldereschi and Meloni[46] (BM) attempted to estimate the parameters x and z via a bond-length versus bond-order correlation, the latter being estimated from the charge densities they calculated in Ref. 23 for the unrelaxed structure. The result is shown as point BM in Fig. 5, and involves only a shift of x away from its ideal value, i.e. the Se atoms move toward the vacancy but remain in the same horizontal plane as in the ideal case. Recently, De Pascale *et al.*[47] (DP) performed a total-energy minimization for α-$CdIn_2Se_4$ using a self-

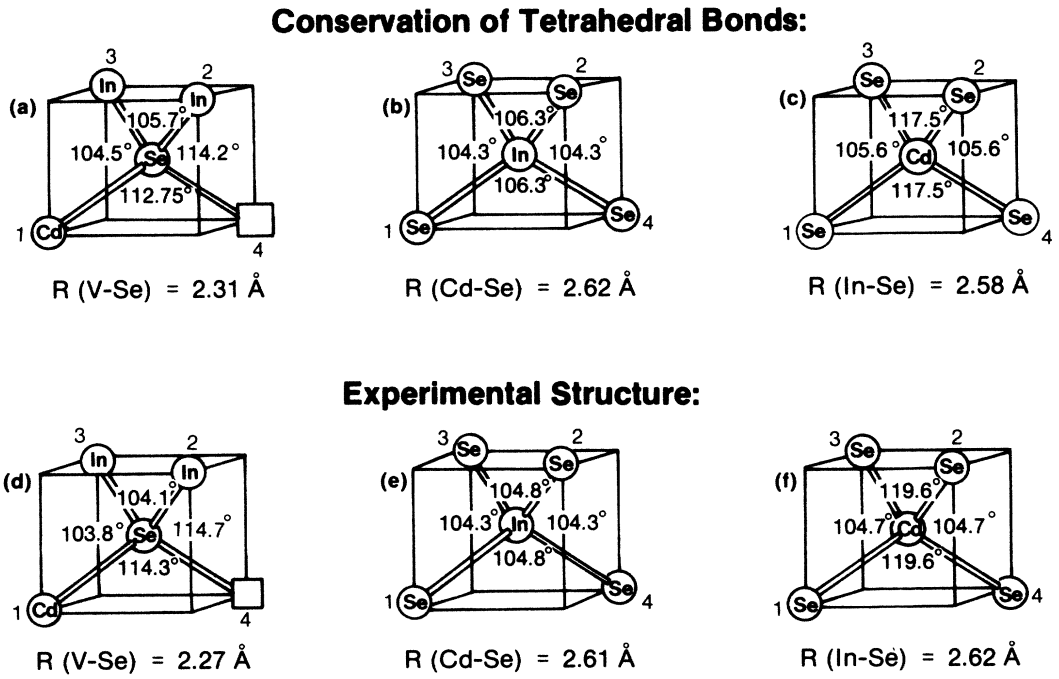

FIG. 4. Bond lengths and bond angles in pseudocubic $CdIn_2Se_4$ determined by the method of conservation of tetrahedral bonds [Eqs. (4) and (5a)] and by the experimental structural refinement of Kawano and Ueda (Ref. 35). A square denotes the vacant site. Angles not explicitly shown are: (a) $\theta_{14}=114.2°$, $\theta_{23}=104.5°$, (b) $\theta_{14}=\theta_{23}=118.3°$, (c) $\theta_{14}=\theta_{23}=105.6°$, (d) $\theta_{14}=114.7°$, $\theta_{23}=103.8°$, (e) $\theta_{14}=\theta_{23}=119.8°$, (f) $\theta_{14}=\theta_{23}=104.7°$, where θ_{ij} indicates the angle formed by sites i and j together with the central atom.

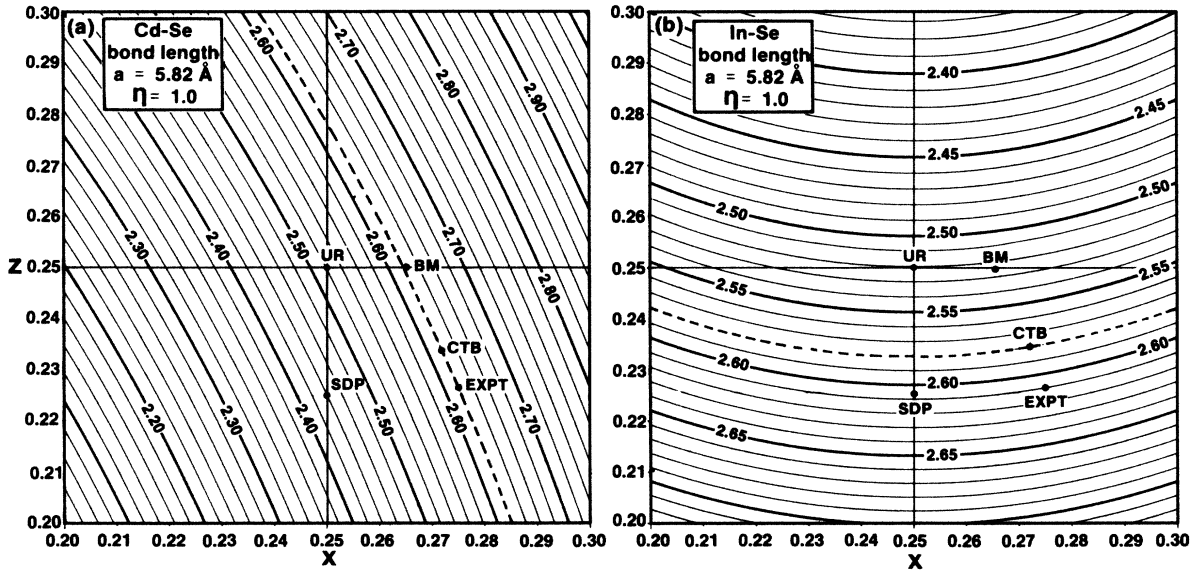

FIG. 5. Bond length contours as a function of the internal parameters, for fixed lattice constant and $\eta=c/a=1.0$ [Eq. (2)]. UR designates the unrelaxed structure, BM the parameters determined by Baldereschi and Meloni (Ref. 46), CTB the parameters determined by the conservation of tetrahedral bonds model [Eq. (4)], SDP the parameters determined by the total-energy-minimization calculation of De Pascal *et al.* (Ref. 47), with the lattice constant scaled to the experimental value, and EXPT designates the experimentally determined parameters of Kawano and Ueda (Ref. 35). The dashed lines indicate the ideal bond lengths as determined by adding the Pauling tetrahedral radii.

TABLE II. Structural parameters (see Fig. 3) of α-$CdIn_2Se_4$ as deduced by various models, compared with the experimental results of single-crystal x-ray data.

Model	a (Å)$=c$ (Å)	x	z	R_{Cd-Se} (Å)	R_{In-Se} (Å)	R_{V-Se} (Å)
Unrelaxed[a] (UR)	5.815	0.25	0.25	2.52	2.52	2.52
Fully Relaxed CTB[b] (FR)	5.815	0.272	0.234	2.62	2.58	2.31
Expt.[c]	5.815	0.275	0.227	2.61	2.62	2.27
BM[d]	5.815	0.265	0.25	2.62	2.52	2.42
DP[e]	5.57	0.25	0.225	2.33	2.49	2.33
Scaled DP[f] (SDP)	5.815	0.25	0.225	2.44	2.60	2.44

[a]Equation (3). Also used by Baldereschi *et al.*, Ref. 23.
[b]Present CTB model, Eqs. (4) and (5a).
[c]Kawano and Ueda, Ref. 35.
[d]Baldereschi and Meloni, Ref. 46.
[e]De Pascale *et al.*, pseudopotential energy minimization (no *d*), Ref. 47.
[f]Same as e, but using experimental lattice parameter.

consistent pseudopotential method but ignoring the cation *d* bands. Their result for the parameter values is shown in Table II as DP. In contrast to the argument of Baldereschi and Meloni,[46] the relaxation found by De Pascale *et al.*[47] involves only a shift of z away from its ideal value, so that the Se atoms move toward the plane containing the vacancy without shifting within their own plane. Note that the value they obtained for the cubic lattice constant (5.57 Å) is about 4% lower than the experimental value.[33–35] The neglect of the Cd *d* orbitals in their calculation is probably the reason for this: Previous attempts[48] to predict equilibrium lattice constants of semiconductor compounds which contain active *d* bands (ZnTe, CdTe, and HgTe) using pseudopotential approaches which *lack d* bands resulted in poor agreement with experiment (e.g., the predicted equilibrium lattice parameters of ZnTe, CdTe, and HgTe were 8%, 10%, and 13%, respectively, too small). Inclusion of *d* states[49] produced very good agreement with experiment. The reason for this[48,49] is understood to be that *d-d* repulsion between the closed-shell *d* states and *p-d* repulsion between the cation *d* band and the anion *p* band, both of Γ_{15} symmetry, increase the equilibrium lattice constant. Hence, it is not surprising that the calculation of De Pascale *et al.* (omitting *d* bands) underestimates (by more than 10%) the Cd—Se bond length, since Cd has shallower *d* bands than In. The results of DP displayed in Fig. 5 have the lattice constant of DP scaled to the experimental value, keeping the same values of the internal parameters ("scaled DP," or SDP, in Table II and Fig. 5).

In what follows we will examine the electronic structure of α-$CdIn_2Se_4$ using three distinct structural models: (i) using the unrelaxed (UR) structure, (ii) using the experimental structure (close to the fully relaxed CTB structure), and (iii) using the scaled pseudopotential structural parameters of De Pascale *et al.* (SDP). The structural parameters are summarized in Table II.

D. Effect of crystal structure on electronic properties

The relaxation of the crystal structure from the equal-bond-length unrelaxed configuration $R_{Cd-Se}=R_{In-Se}=2.51$ Å [Eq. (3)] to the actual, fully relaxed structure with $R_{Cd-Se}=2.61$ Å and $R_{In-Se}=2.62$ Å may affect the electronic properties, in analogy with relaxation around vacancies in binary semiconductors[22] or the anion distortion in chalcopyrites.[40] There has been some controversy in the literature regarding the effect of relaxation on the electronic properties of α-$CdIn_2Se_4$: Baldereschi *et al.*[23,46] observed in the calculated density of states for the *unrelaxed* structure[23] a "valence band gap" of about 0.4 eV at around E_v-1 eV. This gap was not found in photoemission measurements by Picco *et al.*[50] and Margaritondo *et al.*[51] As a consequence, it was speculated[46] that this spurious calculated gap was due to the neglect of the relaxation of the Se sublattice. A later band-structure calculation by Baldereschi and Meloni[46] used estimates (denoted in Table II and Fig. 5 as BM) for the relaxation of x and z away from 1/4. Since the resulting band structure no longer showed evidence of the valence band gap reported in Ref. 23, relaxation has since been assumed to be necessary to obtain realistic band structures. However, it is not obvious that structural relaxation is pertinent: Chizhikov *et al.*[52] found no internal band gap in their band-structure calculation of the *unrelaxed* structure. Similarly, Cerrina *et al.*[53] found strong similarities between the ultraviolet photoemission spectra (UPS) of *pseudocubic* $CdIn_2Se_4$ and *spinel-type* $CdIn_2S_4$, in spite of the latter having a crystal structure quite different from that of the former. Note that the calculations by Baldereschi *et al.*,[23] Baldereschi and Meloni,[46] and Chizhikov *et al.*[52] have all used imperfect structural parameters (Table II and Fig. 5) and ignored the Cd *d* orbitals which, through hybridization with *p* orbitals could broaden valence subbands, hence affect the extent (or existence) of an internal valence band gap. To clarify the situation, we performed self-consistent band-structure calculations for both the unrelaxed and the fully relaxed geometries, retaining the cation *d* orbitals. It will be seen below (Secs. V A and B) that even for the unrelaxed structure our calculation produces no valence band gap.

IV. METHOD OF CALCULATION

The method used in our calculations is the all-electron, potential-variation, mixed-basis (PVMB) approach of

Bendt and Zunger.[54] The crystal potential is represented by the nonrelativistic local-density formalism, using the exchange-correlation functional of Ceperley and Alder,[55] as parametrized by Perdew and Zunger.[56] The explicit inclusion of d orbitals is expected to be significant here, since the Cd 4d states lie within the valence band, and the In 4d states lie just a few eV below the anion s states (see Table III below).

The basis set contains both localized, atomiclike orbitals and plane waves. The localized orbitals are obtained by solving a renormalized-atom problem for each atom, using the same density functional used for the crystal. The atoms are confined to Wigner-Seitz spheres of radii 1.80 Å. The resulting atomic orbitals are then truncated to zero outside nonoverlapping spheres of radii 1.39 Å (Cd and In) and 1.03 Å (Se). The basis is augmented by (symmetrized) plane waves needed to describe the more extended band states.

We have found that little precision is lost if core states deeper than (but not including) Se 3s, and In and Cd 4s are frozen, whereas significant effects (especially on the d levels) may result if some higher states are frozen. Consequently we have frozen the Se $1s2s2p$ states and the Cd and In $1s2s2p3s3p3d$ states. Thus the localized basis set contains nine orbitals for each of Cd, In, and Se. The plane-wave cutoff energy is chosen such that 702 plane waves are included in the basis used for the self-consistent calculations, the total number of basis functions then being 765. Self-consistency in the potential is obtained within a tolerance of 0.1 mRy. The number of fast-Fourier-transform points used to calculate the charge density is 27 000 per cell. The charge density was calculated using one special **k** point at $(0.25,0.25,0.25)2\pi/a$.

V. ELECTRONIC STRUCTURE

A. Band structure and identification of subbands

The Brillouin zone of α-$CdIn_2Se_4$ is shown in Fig. 6 with the high symmetry points and lines labeled. (Reference 57 gives the symmetry properties of this Brillouin zone.) We have calculated band eigenvalues (Table III) at six high symmetry points (directions highlighted by the heavy lines in Fig. 6) and drawn bounds for major groups of bands as shown in Fig. 7 for the UR, the experimental, and the SDP structures. Table IV contains the l-decomposed charge density in spheres centered on each of the atoms for the subbands indicated in Fig. 7.

The band structure of $CdIn_2Se_4$ in the upper ≈ 17 eV range lends itself to a partitioning into subbands, indicated in Fig. 7: (i) the upper valence band, (ii) the In-Se band, (iii) the Cd 4d band, (iv) the Se 4s band, and (v) the In 4d band. This partitioning into five subbands is evidenced in the plots presented in Fig. 8, which show the charge density in the plane defined in Fig. 9(b). [It is necessary to use two different plot planes in order to show the charge density in the vicinity of Cd, In, Se, and the vacancy. We refer to the $(1\bar{1}0)$ plane, containing Cd, Se, and the vacancy, as the *vacancy* plane, and the second plane, $(\bar{1}01)$ if unrelaxed, containing Cd, Se, and In, is referred to as the *indium* plane.]

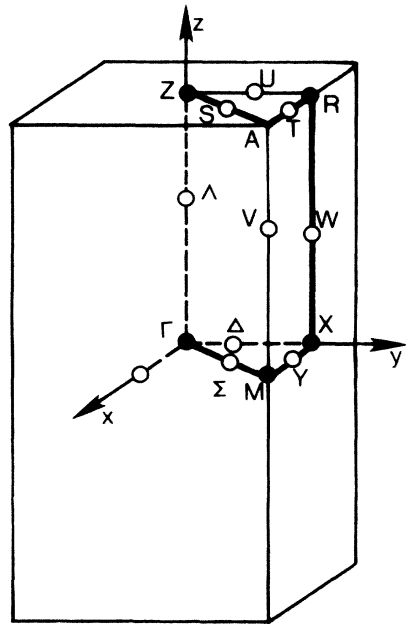

FIG. 6. The Brillouin zone of pseudocubic $CdIn_2Se_4$. Bold lines indicate the directions along which the band structure of Fig. 7 is plotted.

The top $\sim 4-5$ eV region of the valence band, denoted as the "upper valence band", includes mostly Se p states [Fig. 8(a) and Table IV; note also some Cd s and p, and significant In p character in this region]. In general we find that the cation valence electrons (Cd 5s, In 5s and 5p) tend to be concentrated in states toward the lower portion of the upper valence band. A substantial amount of Se p character is found in all of the states in the upper valence band, the amount being smaller in the states with cationlike character near the bottom and dominant in all of the higher states.

Near the bottom of the region labeled *Upper Valence Band* in Fig. 7 one finds one or more states (depending on the **k** point) which have strong In—Se bonding character (dashed area in Fig. 7) exhibiting 59% In s and 30% Se p character (Table IV). A plot of the charge density in the lowest state in this range at the special **k** point is presented in Fig. 8(b), showing clearly the In—Se bond. Jaffe and Zunger[40] found similar behavior in their study of ternary chalcopyrite compounds, including $CuInSe_2$. (There, however, two states were found with this distinctive In—Se bonding character throughout the Brillouin zone.) We hence see that the Cd—Se and In—Se bonds [Figs. 8(a) and 8(b), respectively] originate mostly from distinct energy regions in the band structure.

The identifications of the three narrow bands labeled Cd 4d, Se 4s, and In 4d in Fig. 7 are made clear in Fig. 8, which shows three-dimensional plots of the charge densities at the special **k** point for those bands [Figs. 8(c), 8(d), and 8(e), respectively]. The In 4d and Cd 4d identifications are immediately obvious (see also Table IV), whereas that for the Se 4s group involves other contributions as well: while it has predominantly (78.5%)

TABLE III. Calculated band eigenvalues [in eV, with respect to the valence band maximum (VBM) at Γ] of high-symmetry points (Fig. 6) in α-$CdIn_2Se_4$, for three different structural models (Table II). For the narrow semi-core bands (Cd 4*d* and In 4*d*) only average energies are given. For comparison, the calculated empirical pseudopotential results of Ref. 23 are given for the unrelaxed structure. These were extracted graphically with a precision of 0.1 eV.

	Γ				*M*			
	Ref. 23 UR	UR	Present SDP	Expt.	Ref. 23 UR	UR	Present SDP	Expt.
CBM	1.7[a]	1.06	0.86	1.09	3.5	3.02	3.01	3.29
VBM	0.0	0.00	0.00	0.00	−0.1	−0.25	−0.34	−0.22
	0.0	0.00	0.00	−0.01	−0.1	−0.25	−0.34	−0.22
	−0.1	−0.06	−0.26	−0.02	−1.2	−1.56	−1.37	−0.81
	−1.7	−1.48	−1.51	−1.20	−1.9	−1.61	−1.44	−1.49
	−2.1	−2.01	−1.98	−1.70	−2.2	−1.65	−1.89	−1.94
	−2.1	−2.01	−1.98	−1.70	−2.4	−2.51	−2.35	−2.20
	−2.4	−2.56	−2.60	−2.18	−2.7	−2.53	−2.93	−2.47
	−2.6	−2.57	−2.60	−2.18	−3.2	−2.54	−2.93	−2.47
	−2.6	−2.85	−2.86	−2.55	−3.2	−3.19	−2.99	−2.61
	−2.9	−2.96	−3.12	−3.35	−3.7	−3.74	−3.96	−3.52
	−4.7	−5.12	−5.32	−4.62	−4.7	−5.09	−4.88	−4.67
	−5.3	−5.91	−5.56	−5.32	−4.7	−5.10	−4.89	−4.68
⟨Cd *d*⟩		−9.37	−9.50	−9.07		−9.42	−9.54	−9.08
Se *s*	−14.7	−11.71	−11.90	−11.33	−14.7	−11.79	−11.93	−11.30
	−15.4	−11.71	−11.90	−11.33	−14.8	−11.82	−12.06	−11.72
		−11.72	−12.01	−11.43		−12.21	−12.30	−11.79
		−12.93	−12.89	−12.53		−12.21	−12.30	−11.79
⟨In *d*⟩		−16.06	−16.07	−15.81		−16.07	−16.05	−15.79
	X				*R*			
	Ref. 23 UR	UR	Present SDP	Expt.	Ref. 23 UR	UR	Present SDP	Expt.
CBM	3.5	3.31	3.06	3.01	2.6	3.53	2.91	3.34
VBM	−0.3	−0.67	−0.65	−0.64	0.1	−0.36	−0.45	−0.45
	−0.4	−0.69	−0.96	−0.90	0.1	−0.46	−0.59	−0.47
	−1.0	−1.35	−1.48	−1.09	0.0	−1.05	−1.03	−0.53
	−1.9	−1.59	−1.50	−1.12	−1.7	−1.22	−1.24	−1.04
	−2.1	−1.59	−1.68	−1.65	−1.8	−1.66	−1.91	−1.87
	−2.1	−2.34	−2.41	−2.16	−1.8	−2.44	−2.39	−2.17
	−3.0	−2.99	−2.76	−2.47	−2.1	−2.61	−2.41	−2.43
	−3.0	−3.01	−2.97	−2.67	−2.1	−2.70	−2.76	−2.49
	−3.3	−3.17	−3.25	−2.95	−2.6	−3.56	−3.46	−2.95
	−3.5	−3.32	−3.31	−3.06	−4.4	−4.30	−4.30	−3.83
	−4.5	−4.69	−4.59	−4.50	−5.1	−4.73	−4.62	−4.52
	−4.8	−5.19	−5.16	−4.53	−5.1	−5.03	−5.06	−4.57
⟨Cd *d*⟩		−9.40	−9.51	−9.07		−9.41	−9.53	−9.07
Se *s*	−14.7	−11.70	−11.93	−11.32	−14.9	−11.71	−11.96	−11.47
	−15.0	−11.72	−11.98	−11.43	−14.9	−11.83	−12.07	−11.59
		−12.34	−12.40	−11.85		−12.25	−12.26	−11.74
		−12.37	−12.40	−12.08		−12.26	−12.32	−11.83
⟨In *d*⟩		−16.07	−16.06	−15.80		−16.06	−16.06	−15.79

Se *s* character, it also has a non-negligible amount (9.1%) of Cd *d* character and a lesser amount (5.2%) of In *d* character (Table IV). The mixing of this large amount of Cd *d* character with Se *s* character results in noticeable Cd-Se bonding in these states, as can be seen from Fig. 8(d).

B. Comparison with pseudopotential studies

Baldereschi *et al.*,[23] have studied the properties of unrelaxed $CdIn_2Se_4$ using a local, empirical pseudopotential method.[58] Their results are compared with those obtained here for identical structural parameters in Table III,

TABLE III (*continued*).

	A			*Z*		
	UR	Present SDP	Expt.	UR	Present SDP	Expt.
CBM	1.86	1.54	1.90	2.81	2.75	2.95
VBM	−0.24	−0.35	−0.26	−0.62	−0.78	−0.62
	−0.24	−0.35	−0.26	−0.62	−0.78	−0.62
	−0.27	−0.36	−0.38	−1.41	−1.66	−1.36
	−1.04	−0.90	−0.50	−1.94	−1.66	−1.36
	−1.19	−1.29	−0.97	−1.94	−1.67	−1.81
	−1.19	−1.34	−0.97	−2.24	−2.11	−1.91
	−1.54	−1.35	−1.00	−2.75	−2.86	−2.47
	−1.65	−1.44	−1.23	−2.75	−2.86	−2.47
	−3.45	−3.60	−3.59	−3.43	−3.49	−3.24
	−5.02	−5.06	−4.55	−3.44	−3.61	−3.36
	−5.78	−5.71	−5.39	−3.67	−3.92	−3.40
	−5.79	−5.72	−5.39	−5.80	−5.36	−5.08
⟨Cd *d*⟩	−9.38	−9.49	−9.04	−9.41	−9.53	−9.08
Se *s*	−11.68	−11.82	−11.45	−11.72	−11.90	−11.32
	−11.85	−12.08	−11.53	−11.72	−11.90	−11.32
	−12.20	−12.30	−11.78	−11.89	−12.21	−11.80
	−12.21	−12.30	−11.78	−12.74	−12.64	−12.20
⟨In *d*⟩	−16.06	−16.05	−15.79	−16.07	−16.06	−15.79

[a]Value adjusted to the then-accepted experimental data.

showing an overall similarity with our results for the same unrelaxed geometry. To gain some insight into the differences, we briefly review some of the pertinent aspects of the method used by these authors.

In their study, *d* bands are ignored and the *i*th atom nonlocal bare ion pseudopotential (different, in general, for *s* and *p* electrons) is replaced by a local potential (common to *s* and *p* electrons) of the form

$$V_{\text{ion}}^{(i)}(r)=\frac{\alpha_i e^{\beta_i r^2}}{r}\sin(\gamma_i r)-\frac{2Z_i^*}{r} , \tag{6}$$

where $i=$ Cd, In, Se. This potential is screened (in a momentum representation) by a phenomenological dielectric function[58] in which the dielectric constant ϵ_0 is taken as the average over the constituents. The constants $(\alpha_i, \beta_i, \gamma_i)$ are first adjusted for each atom type i by fitting observed transitions in elemental semiconductors (Si, Ge, Sn), and then adjusted by fitting data on binary semiconductors, retaining smooth regularities of those parameters across the Periodic Table. Z_i^* is the *effective* number of valence electrons, deviating from the *nominal* valence (e.g., 2, 3, and 6 for Cd, In, and Se, respectively) by the charge-transfer term ΔZ_i:

$$Z_i^*=Z_i\pm\Delta Z_i , \tag{7}$$

where the + and − signs refer to cations and anions, respectively. Electroneutrality requires that

$$\sum_i N_i\Delta Z_i=0 , \tag{8}$$

where N_i is the number of atoms of type i in the formula unit. The $\{\Delta Z_i\}$ values are adjusted empirically to fit the band gap of the *ternary* system being studied. ΔZ_i hence depends both on the atom type i and on the compound to which this atom belongs. The band structure is calculated non-self-consistently for a fixed set of dielectrically screened ionic potentials, using a small set of plane wave

TABLE IV. *l*-decomposed charge in atomic spheres for the five groups of bands shown in Figs. 7 and 8 (experimental structure). Values are given as a percentage of the total charge in atomic spheres for all orbitals in the group. The percentage of the total charge which lies within the atomic spheres is shown in the last column for each group.

	Cd			In			Se			Total
	s	*p*	*d*	*s*	*p*	*d*	*s*	*p*	*d*	
UVB	4.4	4.1	2.4	6.4	11.9	2.4	3.0	65.1	0.3	46.0
In–Se	0.0	0.9	1.7	59.0	2.5	0.6	4.5	30.3	0.5	53.3
Cd 4*d*	0.0	0.0	95.8	0.3	0.2	0.2	2.8	0.6	0.1	93.6
Se 4*s*	0.9	0.8	9.1	3.0	2.1	5.2	78.5	0.4	0.0	63.9
In 4*d*	0.0	0.0	0.0	0.0	0.0	99.1	0.7	0.1	0.0	97.2

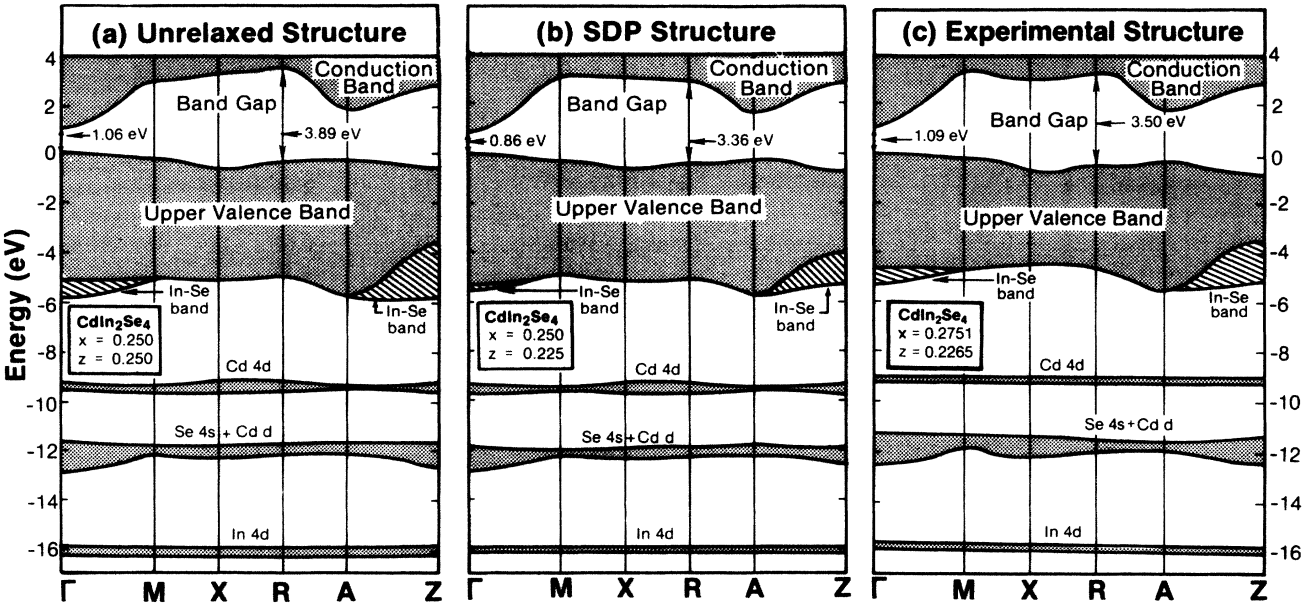

FIG. 7. Band structures calculated at six high-symmetry points for (a) the unrelaxed structure, (b) the scaled De Pascale structure, and (c) the experimental structure. All were calculated at a lattice constant of $a=5.815$ Å. Rather than show the complex bands within each subband, we delineate the regions of the main groups of bands.

basis functions. Since band gaps increase with ionicity, large $|\Delta Z_i|$ values are needed to fit materials with larger band gaps, e.g. $\Delta Z_{Se}(CdIn_2Se_4)=-0.65e$, but $\Delta Z_{Se}(ZnSe)=-1.25e$ is needed to fit the larger gap of ZnSe. For $CdIn_2Se_4$, they use $\Delta Z_{Cd}=+1.2e$, $\Delta Z_{In}=+0.7e$, and $\Delta Z_{Se}=-0.65e$ [$N_{Cd}=1$, $N_{In}=2$, and $N_{Se}=4$ in Eq. (8)], to fit the measured band gap. Since the dielectric screening used is not self consistent with $V_{ion}(r)$ of Eq. (6), all atoms are screened nearly equally. This leaves a net strong attractive (repulsive) potential on the Se (Cd, In) sites, on account of the negative (positive) ΔZ_i's.

Comparing the results for the band structure of unrelaxed $CdIn_2Se_4$ of Baldereschi *et al.*,[23] with the present results (Table III), we note the following differences.

(i) The pseudopotential model underestimates the width of the upper valence band by ~ 0.5 eV, i.e. it does not exhibit the extra width associated with the In-Se band at the bottom of the upper valence band (cross-hatched area in Fig. 7). This is consistent with the use of a strongly repulsive In potential in the work of Baldereschi *et al.*, shifting states associated with In to less negative energies.

(ii) The pseudopotential model overestimates by ~ 2 eV the binding energy of the Se 4*s* band (Table III). This is consistent with their use of an overly attractive ionic Se potential, and is further evidenced by the accumulation of substantial electron density on the Se sites in their calculation (Fig. 3 in Ref. 23), at the expense of a nearly complete depletion of electronic charge from the Cd and In sites (compare the present charge density in Fig. 10 below).

(iii) The direct band gap in the pseudopotential calculation (1.7 eV, fit to experiment by adjusting the ΔZ_i's) is considerably larger than that obtained in our nonempirical study here (1.06 eV in Table III). Since the valence band maximum has mostly anion character, whereas the conduction band minimum has cation character, empirical adjustment[23] of $\delta Z=|\Delta Z_{cation}-\Delta Z_{anion}|$ increases this band gap toward its experimental value. The smaller band gap obtained here in the first-principles local-density model has its origin in the imperfect correlation energy[56] underlying the local density approach. In the pseudopotential model,[23,46] this physical effect is circumvented by using an empirically adjusted enhanced ionicity (δZ).

(iv) Whereas the pseudopotential calculation shows a valence-band gap from $\sim E_v-1.1$ eV to $\sim E_v-1.5$ eV (Table III), our calculation shows that there are states in this energy range even in the unrelaxed model, at the symmetry points *X*, *R*, and *A* (Table III). This is consistent with the inclusion of Cd *d* states in the present calculation: through hybridization with the anion *p* states, these broaden the valence band and eliminate the valence-band gap. Recall that no valence-band gap is in evidence in the photoemission data.[50,51]

(v) The valence-to-conduction band gap shown in Fig. 7 is direct at Γ, for both the unrelaxed and relaxed structures. This is in contrast to the calculation of Baldereschi *et al.*,[23] who found the maximum of the valence band at the *R* point (they did not calculate the *A* and *Z* points). However, they found that the top of the valence band was exceptionally flat (more so than in our Fig. 7), and they expressed some uncertainty about the reliability of that prediction. The band structure calculated by Chi-

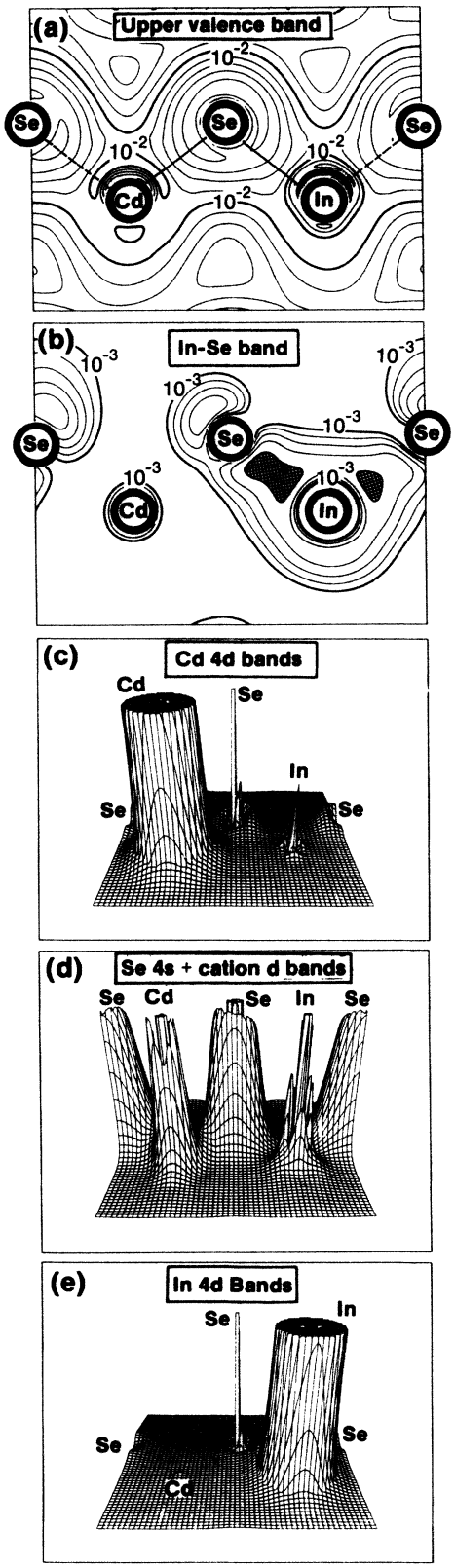

FIG. 8. Charge densities for the five major groups of bands appearing in the band structures of Fig. 7. The densities were calculated at a single special **k** point. Contour spacings are logarithmic with values in electrons per a.u.^{3} shown for every fifth contour.

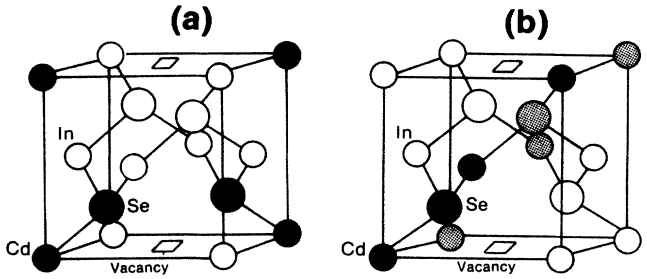

FIG. 9. Plot planes used for charge density plots. (a) shows the *vacancy* plane, which includes the solid atoms and the vacancies, and (b) shows the *indium* plane, the solid atoms being in the plane for all values of the structural parameters x and z, and the grey atoms being in the plane only for the unrelaxed values of the parameters.

zhikov *et al.*[52] also shows an indirect gap, but the valence band maximum is at A rather than at R, the Γ point is higher in energy than the R point, and the difference in energy between the A and Γ points is only 0.07 eV. Thus, it is clear that the details of the top of the valence band are quite sensitive to the details of the method of calculation, though our calculation suggests that the dependence on the internal parameters of the structure (x and z) is relatively weak.

C. Relaxation effects on the band structure

Table III and Fig. 7 show only subtle changes in the electronic structure with relaxation. From Table II we see that the main effect of relaxation is to increase *both* the Cd—Se and In—Se bond lengths by ~ 0.1 Å. This relaxation has a similar effect on the valence and conduction bands, leaving the direct gap virtually unchanged. Relaxation reduces, however, the width of the upper valence band by ~ 0.6 eV, reflecting the fact that the In-Se band is *bonding* (see Fig. 8); hence, increasing the bond length upon relaxation raises its energy and narrows thereby the upper valence band. Indeed, most of the (bonding) states associated with the upper valence band move to higher energies as the two primary bond lengths increase (Table II). Similarly, the (bonding) Cd 4*d* and In 4*d* bands move up by 0.3 eV and 0.2 eV, respectively, responding to an increase in bond lengths. This increase in bond lengths reduces the dispersion of the Cd 4*d* band [Fig. 7(c)].

D. Total charge densities

The total charge density in all states above and including In 4*d* is shown in Fig. 10 in both planes depicted in Fig. 9. The contours are logarithmically spaced; the contour levels are given in electrons per cubic a.u. The plot in the vacancy plane [Fig. 9(a)] shows that the amount of charge at the vacant site is quite small. The plots show clearly the Cd-Se and In-Se bonding. However, in comparison with the results of Baldereschi *et al.*,[23,46,58] these bonds appear to be less ionic, the metal sites have considerably more charge (on account of their *d* states) and no

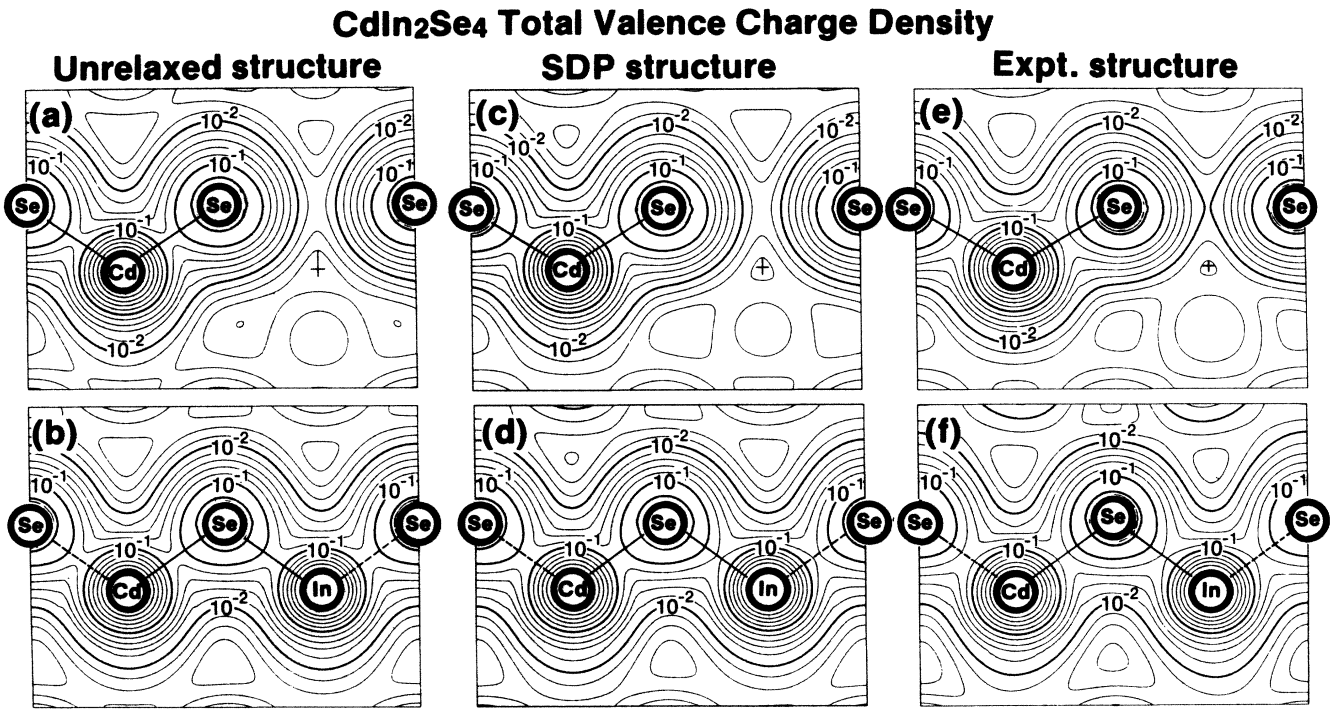

FIG. 10. Total valence charge densities shown in both the vacancy plane [(a), (c), and (e), see Fig. 9(a)], and the indium plane [(b), (d), and (f), see Fig. 9(b)] for the unrelaxed [(a) and (b)], scaled De Pascale [(c) and (d)], and experimental [(e) and (f)] structures. Contour spacings are logarithmic with values in electrons per a.u.^{3} shown for every fifth contour. Solid straight lines denote bonds in the planes, dashed straight lines denote bonds which are not exactly in the plane for the relaxed structures [(c)–(f)]. Note the very low charge density at the vacancy (indicated by a cross) and the lack of evidence of a lone pair oriented toward the vacancy.

evidence is found for metalliclike Cd—In bonds [see Fig. 7 in Ref. 58(b)]. *There is little evidence of any perturbation of the charge density around the Se atoms in the direction of the vacancy.* Hence, the expected lone pair appears to have been distributed over the adjacent (to the vacancy) atoms and their bonds rather than occupying the space near the vacancy. The appearance of the contours in the indium plane, in particular, is quite similar to that seen in a binary, zinc-blende compound.[24,25,54]

E. Dangling bonds and lone pairs in the upper valence band

To examine in detail the fact that the lone pair appears to be distributed, we show plots of six of the seven uppermost valence states at Γ in Fig. 11 in the vacancy plane [Fig. 9(a)]. [The state at -2.86 eV (the sixth of the seven) has less charge density than the threshold for the lowest contour, so it is omitted.] In these plots one sees states with mainly Se p character, often with dangling orbitals. These occur in a variety of orientations, not necessarily directed toward the vacancy. The spread in energy of these states is relatively large (about 3 eV). It is the variety of orientations, together with the fact that none of these states has a significant amount of charge at the vacant site, that is responsible for the lack of evidence of a lone pair in the total valence density. We conclude that the anionlike lone-pair dangling bonds are spread in $CdIn_2Se_4$ into a broad band.

F. X-ray scattering factors

The differences between the charge distributions in the various structural models become apparent when their Fourier transforms are contrasted. These differences may be of some use in distinguishing the relaxed from the unrelaxed structures and in distinguishing the completely ordered structure from various possible disordered structures with the same composition. To this end, we present in this section an analysis of the x-ray scattering factors for the ordered structure and several possible disordered structures, together with a comparison with the experimentally determined x-ray scattering factors of Kawano and Ueda.[35]

We calculate from the total charge density of the crystal,

$$\rho(\mathbf{r})=\sum_n \sum_{\mathbf{k}} N_{n\mathbf{k}} \mid \psi_{n\mathbf{k}} \mid^2 , \tag{9}$$

where $\psi_{n\mathbf{k}}$ is the wave function for band n and wave vector $\mathbf{k}$, and $N_{n\mathbf{k}}$ is the corresponding occupancy, the Fourier transform

$$\rho_{\text{calc}}(\mathbf{G})=\int \rho(\mathbf{r}) e^{-i\mathbf{G}\cdot\mathbf{r}} d\mathbf{r} , \tag{10}$$

where $\mathbf{G}$ is a reciprocal-lattice vector. The measured x-ray scattering factor includes the Fourier transform $\rho_{\text{expt}}(\mathbf{G})$ as well as temperature and other factors, i.e.,

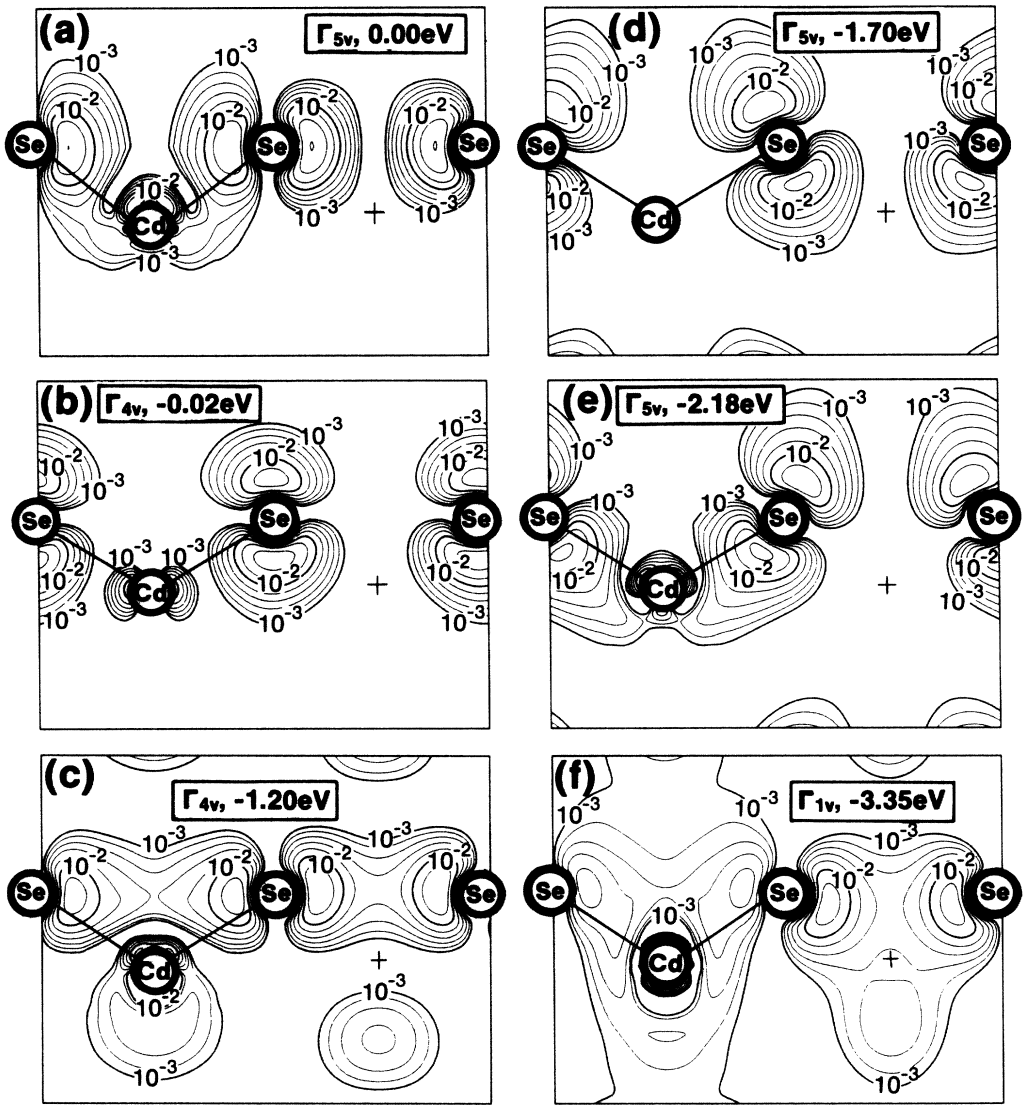

FIG. 11. Square of the wave-function amplitude for six of the highest seven bands at Γ. Contour spacings are logarithmic with values in electrons per a.u.^{3} shown for every fifth contour, and the vacant site is indicated by a cross. Here there is evidence for lone-pair-like states, but their orientations are varied, thus explaining the reason for the lack of evidence of lone-pair states in the total charge densities shown in Fig. 10.

$$F_{\text{expt}}(\mathbf{G},T)=\rho_{\text{expt}}(\mathbf{G})g(\mathbf{G},T)\ . \tag{11}$$

One can model $\rho_{\text{expt}}(\mathbf{r})$ as a superposition of atomic charge densities $\rho_\alpha(\mathbf{r})$ of atoms of type α

$$\rho_{\text{sup}}(\mathbf{r})=\sum_n\sum_i\rho_{\alpha_i}(\mathbf{r}-\mathbf{R}_n-\tau_i)\ , \tag{12}$$

where $\mathbf{R}_n$ are direct lattice vectors of unit cell n, and τ_i are the site vectors of the atom at site i. The Fourier transform is then

$$\begin{aligned}\rho_{\text{sup}}(\mathbf{G})&=\int\rho_{\text{sup}}(\mathbf{r})e^{-i\mathbf{G}\cdot\mathbf{r}}d\mathbf{r}\\&=N\sum_i\rho_{\alpha_i}(\mathbf{G})e^{-i\mathbf{G}\cdot\tau_i}d\mathbf{r}\ ,\end{aligned} \tag{13}$$

where

$$\rho_\alpha(\mathbf{q})=\int\rho_\alpha(\mathbf{r})e^{-i\mathbf{q}\cdot\mathbf{r}}d\mathbf{r}\ , \tag{14}$$

and N is the number of primitive unit cells in the crystal. It is usual in structural refinement to use spherical atomic charge densities $\rho_\alpha(|\mathbf{r}|)$ to get atomic form factors

$$f_\alpha(q)=\int\rho_\alpha(|\mathbf{r}|)e^{-i\mathbf{q}\cdot\mathbf{r}}d\mathbf{r}\ , \tag{15}$$

which depend only on $q=|\mathbf{q}|$, and to calculate $\rho(\mathbf{G})$ only for a single cell, so that $\rho(\mathbf{0})$ is just the number of electrons per primitive cell [i.e., divide Eq. (13) by N]. In the study of Kawano and Ueda $f_\alpha(q)$ could be taken as the Thomas-Fermi-Dirac atomic form factors available at the time.[59]

To compare our calculated $\rho_{\text{calc}}(\mathbf{G})$ with $\rho_{\text{expt}}(\mathbf{G})$ we need to remove $g(\mathbf{G},T)$ from the measured data, $F_{\text{expt}}(\mathbf{G},T)$. We do so via the expression

$$\rho_{\text{expt}}(\mathbf{G})=F_{\text{expt}}(\mathbf{G})\frac{\rho_{\text{sup}}(\mathbf{G})}{F_{\text{sup}}(\mathbf{G})}, \tag{16}$$

where $F_{\text{expt}}(\mathbf{G})$ represents the raw experimental data given by Kawano and Ueda,[35] and $F_{\text{sup}}(\mathbf{G})$ is the equivalent structure factor calculated by Kawano and Ueda from atomic form factors together with corrections for temperature and other factors [their model for $g(\mathbf{G},T)$], and $\rho_{\text{sup}}(\mathbf{G})$ is calculated from atomic form factors obtained from spherical Thomas-Fermi-Dirac charge densities.[59] As can be seen from Eqs. (9) and (10), we do not use a spherical superposition approximation in our first-principles calculation, whereas the analysis of the data by Kawano and Ueda does involve this (routine) approximation.

To gain insight into the selection rules governing the x-ray scattering factors, we calculated $\rho_{\text{sup}}(\mathbf{G})$ analytically using Eq. (13) (with the assumption of spherical atomic form factors), and the atomic positions of the $CdIn_2Se_4$ structure [Eq. (1)]. The x-ray structure factor for the ordered unit cell is then

$$\rho_{\text{sup}}(\mathbf{G})=f_A+f_V e^{-i\pi(h+k)}+f_B e^{-i\pi\eta l}(e^{-i\pi h}+e^{-i\pi k}) +f_C f(x,z,h,k,\eta l) \tag{17}$$

where

$$\begin{aligned} f(x,z,h,k,\eta l)=&e^{-i(\pi/2)[4x(h+k)+4z\eta l]} \\ &+e^{-i(\pi/2)[-4x(h+k)+4z\eta l]} \\ &+e^{-i(\pi/2)[4x(h-k)-4z\eta l]} \\ &+e^{-i(\pi/2)[-4x(h-k)-4z\eta l]}. \end{aligned} \tag{18}$$

Here h, k, and l are Miller indices along Cartesian axes (h, k, and ηl are integers); x, z, and η are the structural parameters [Eqs. (1) and (2)]; and the f_α are atomic structure factors of Eq. (15). The subscripts A, B, and C refer to the atoms in a cell with the formula $A^{\text{II}}B_2^{\text{III}}C_4^{\text{VI}}V$, and V indicates the site normally vacant in the $CdIn_2Se_4$ structure. It is clear from Eqs. (17) and (18) that there are no forbidden reflections for the ordered structure.

The value of f_V in Eq. (17) is essentially zero when that site is vacant; however, several types of disorder on the cation sublattice are possible (Sec. III A), and it will be useful to carry along the structure factor for the nominally vacant site in order to examine the effects of some of these. Consider two of the possible types of disorder on the cation sublattice: (i) random exchange of the Cd atoms A with the vacancies V, and (ii) completely random placement of Cd (A), In (B), and vacancies (V) on the sites of the cation sublattice. In case (i) the result is a virtual CuAu I superlattice-type structure [Fig. 1(a)], denoted $\langle AV\rangle B_2Se_4$ (where $\langle\ \rangle$ indicates disorder on the sites occupied by the enclosed species), the reflections of which have been discussed previously.[60,61] Case (ii) results in a virtual zinc-blende lattice $\langle AB_2V\rangle Se_4$ [Fig. 1(j)]. With these two types of disorder in mind, we divide the reflections of the $CdIn_2Se_4$ structure into three classes. These will be referred to as class 1, zinc-blende-allowed reflections; class 2, zinc-blende-forbidden reflections, and class 3, CuAu I–forbidden reflections. Class 1 consists of those reflections which satisfy the zinc-blende reflection condition that h, k, and ηl are all odd or all even. Class 2 contains those reflections which satisfy the reflection condition for the CuAu I–type superlattice structure but do not satisfy the zinc-blende reflection condition (all zinc-blende-allowed reflections are also CuAu I allowed). The condition is that $h+k$ is even and $h+\eta l$ (as well as $k+\eta l$) is odd. Class 3 contains those reflections of the $CdIn_2Se_4$ structure that are not in classes 1 or 2, specifically those for which $h+k$ is odd. These are the reflections whose presence distinguishes the $CdIn_2Se_4$ structure from the zinc-blende [Fig. 1(j)] and the CuAu I–type [Fig. 1(a)] superlattice structures. Table V summarizes the classification of the x-ray reflections, showing the forms of the contributions due to the cation sublattice and the anion sublattice separately. The simplification in the contribution due to the anion sublattice as the internal parameters x and z approach the unrelaxed (1/4) values is also shown.

Consider the effects of the two types of disorder discussed above. If there is random exchange of the Cd atoms with vacancies, the cation contribution to the class 3 reflections vanishes. Since the virtual crystal which represents the structure with this type of disorder has an average distortion parameter near $\langle x\rangle = 1/4$, the anion

TABLE V. Classification of x-ray reflections of the $CdIn_2Se_4$ structure. ρ_c and ρ_a are the contributions from the cation and anion sublattices, respectively. The generic formula is AB_2C_4V, where A, B, C, and V represent the sites occupied by Cd, In, Se, and the vacancy, respectively. The f_α ($\alpha = A$, B, C, or V) are atomic structure factors. The general form of the function f is given in Eq. (18).

	Class 1 Zinc-blende allowed h, k, ηl all even, all odd	Class 2 Zinc-blende forbidden $h+k$ even, $h+\eta l$ odd	Class 3 CuAu-I forbidden $h+k$ odd
x arb. z arb. (expt)	$\rho_c=f_A+f_V+2f_B$ $\rho_a=f_C f(x,z,h,k,\eta l)$	$\rho_c=f_A+f_V-2f_B$ $\rho_a=f_C f(x,z,h,k,\eta l)$	$\rho_c=f_A-f_V$ $\rho_a=f_C f(x,z,h,k,\eta l)$
$x=1/4$ z arb. (SDP)	$\rho_c=f_A+f_V+2f_B$ $\rho_a=f_C f(1/4,z,h,k,\eta l)$	$\rho_c=f_A+f_V-2f_B$ $\rho_a=f_C f(1/4,z,h,k,\eta l)$	$\rho_c=f_A-f_V$ $\rho_a=0$
$x=1/4$ $z=1/4$ (UR)	$\rho_c=f_A+f_V+2f_B$ $\rho_a=4f_C e^{-i\frac{\pi}{2}(h+k+\eta l)}$	$\rho_c=f_A+f_V-2f_B$ $\rho_a=0$	$\rho_c=f_A-f_V$ $\rho_a=0$

contribution vanishes as well, and no class 3 reflections should be observed if this type of disorder exists in the sample. If the placement of the cations and vacancies on the cation sublattice is completely random, the cation contribution to both classes 2 and 3 vanishes. In this case the virtual crystal is zinc-blende, having $<x>=<z>=1/4$, so the anion contributions to all reflections in classes 2 and 3 also vanish, leaving only the zinc-blende-allowed reflections to be observed.

In addition to these types of disorder, there is the possibility of random placement of the Cd and In atoms on the sites normally occupied by these atoms [the stage-I disorder of Sec. III A and Fig. 1(h)]. The symmetry of the stage-I disordered structure is the same as that of the Cu_3Au-like structure shown in Fig. 1(b), for which the x-ray scattering factors are

$$\rho_{\rm sup}(\mathbf{G})=f_A+f_B(e^{-i\pi(h+k)}+e^{-i\pi(k+l)}+e^{-i\pi(l+h)}) +f_C f(x,h,k,l)\ , \tag{19}$$

where

$$f(x,h,k,l)=e^{-i(\pi/2)[4x(h+k+l)]} +e^{-i(\pi/2)[4x(-h-k+l)]} +e^{-i(\pi/2)[4x(h-k-l)]} +e^{-i(\pi/2)[4x(-h+k-l)]}. \tag{20}$$

For the stage-I disordered structure, replace atom A by a vacancy and atom B by an "averaged" cation. There are no forbidden reflections for this structure, so it is not possible to distinguish this state from the ordered one by the mere presence or absence of certain reflections. However, there are differences in the patterns of the degeneracies to be expected, and we examine these next.

The degeneracies of the x-ray scattering factors of the completely ordered structure, Eqs. (17) and (18) and Table V, are listed below. Some of these degeneracies hold only for special values of the parameters x and z.

(i) $\rho_{\rm sup}$ is degenerate under permutation of the indices h and k. As a consequence, the numerical values we report later will include only one of each pair $(h,k,\eta l)$ and $(k,h,\eta l)$.

(ii) If $|x-0.25|=|z-0.25|$ (including but not limited to the case $x=z$) then reflections in class 1 are invariant under all possible permutations of the quantities h, k, and ηl, and reflections in class 3 are invariant under just one of the permutations $h\leftrightarrow\eta l$ or $k\leftrightarrow\eta l$. The other permutation interchanges reflections in classes 2 and 3 and does not preserve the intensity.

(iii) If $x=z=0.25$ then within each class all reflections with the same $|\mathbf{G}|$ are degenerate. This degeneracy does not cross classes, i.e., reflections having the same $|\mathbf{G}|$ but belonging to different classes are not degenerate.

The reflections of the stage-I-disordered structure, Eqs. (19) and (20) are degenerate under all permutations of the indices h, k, and l for all values of the parameter x. Therefore, violations of this degeneracy can be taken as an indication of a higher degree of order than that of the stage-I-disordered structure.

It is clear from the analysis of the degeneracies of the ordered structure that the degeneracy pattern can also be used to quickly distinguish relaxed structures from the unrelaxed structure.

We present in Table VI our calculated x-ray scattering factors for both the unrelaxed and relaxed structures, along with a list of values obtained from the experimental data published by Kawano and Ueda[35] by correcting for temperature (Debye-Waller) and other factors according to Eq. (16). An examination of Table VI in light of our earlier discussions based on the analytical expressions for the scattering factors yields several observations.

(i) The presence of relatively strong class 2 and class 3 reflections in the experimental data suggests that both random interchanges of Cd and vacancies and stage-II disorder are not present (at least in a dominant way) in the sample used by Kawano and Ueda.

(ii) The lack of degeneracy under general permutations of h, k, and l indicates that the amount of stage-I disorder may be small as well; indeed, those near degeneracies which are present parallel very closely those present in the completely ordered structure [the calculated $\rho_{\rm R}(\mathbf{G})$ in Table VI]. However, the near degeneracies present in the class 1 and class 3 reflections of the completely ordered structure are due to the near equality of the differences between the internal parameters x and z and their unrelaxed values, specifically, $|x-0.25|=0.0251$ and $|z-0.25|=0.0235$, as well as to the similarity in the atomic form factors of Cd and In. Since the breaking of the degeneracy is relatively small even in the completely ordered structure, we cannot use this criterion to rule out with certainty the presence of stage-I disorder.

(iii) The breaking of the degeneracies of the unrelaxed structure [$\rho_{\rm UR}(\mathbf{G})$ in Table VI] in both the calculated values, $\rho_{\rm R}(\mathbf{G})$, and the corrected experimental values, $\rho_{\rm expt}(\mathbf{G})$, indicates clearly the presence of relaxation of the internal parameters. An example is the breaking of the degeneracy of the [212] and [300] reflections in class 3.

(iv) The small violations of the analytically derived degeneracies for the unrelaxed structure, of the order of 0.1, are a result of breakdown of the validity of the analytic forms [Eqs. (17)–(20)], which are superpositions of spherical atomic form factors. The first principles calculation, the results of which are reported in Table VI, does not assume that the crystal density can be expressed as a superposition of spherical atomic charge densities. What is remarkable is that the superposition approximation appears to be so good.

We have computed the R factors,

$$R=\frac{\sum \big|\,|\rho_{\rm expt}|-|\rho_{\rm calc}|\,\big|}{\sum|\rho_{\rm expt}|}\ , \tag{21}$$

relating the fit of our calculated x-ray scattering factors to the corrected experimental scattering factors for each of the three sets of structural parameters for which we have evaluated the first-principles charge density and find the following values: 0.257 (unrelaxed structure), 0.200 (SDP structure), and 0.073 (experimental structure of Kawano and Ueda). These values were calculated using

TABLE VI. Comparison of x-ray reflections of the $CdIn_2Se_4$ structure. $|\mathbf{G}|$ is in units of $2\pi/a$, where a is the lattice constant. The classes are defined in Table V. The subscripts UR, R, and expt refer to the unrelaxed structure, the relaxed structure, and the corrected experimental data of Kawano and Ueda,[35] respectively. See Eq. (16) for the method used to determine $\rho_{expt}(\mathbf{G})$.

Class 1 reflections					Class 2 reflections				
hkl	$\lvert G \rvert$	$\rho_{UR}(\mathbf{G})$	$\rho_R(\mathbf{G})$	$\rho_{expt}(\mathbf{G})$	*hkl*	$\lvert G \rvert$	$\rho_{UR}(\mathbf{G})$	$\rho_R(\mathbf{G})$	$\rho_{expt}(\mathbf{G})$
000	0.00	282.0	282.0	282.0	001	1.00	47.0	28.1	34.2
111	1.73	172.8	170.3	165.5	110	1.41	44.6	41.7	45.9
002	2.00	9.9	14.7	26.6	201	2.24	40.6	55.9	50.3
200	2.00	9.9	15.5	20.9	112	2.45	39.7	51.6	48.7
220	2.83	210.4	200.7	189.0	221	3.00	36.9	25.6	0.0
202	2.83	210.5	201.3	185.8	003	3.00	36.9	79.0	69.1
311	3.32	139.6	130.8	123.2	310	3.16	36.2	43.1	36.9
113	3.32	139.6	131.5	124.0	203	3.61	34.1	3.0	0.0
222	3.46	8.7	21.5	0.0	312	3.74	33.6	35.9	34.5
400	4.00	180.9	164.2	150.9	401	4.12	31.9	21.7	0.0
004	4.00	180.9	166.2	153.8	223	4.12	32.1	65.7	69.3
331	4.36	122.6	113.2	112.6	330	4.24	31.4	13.9	0.0
313	4.36	122.6	113.7	115.2	114	4.24	31.4	54.7	49.1
204	4.47	6.5	23.8	30.9	421	4.58	30.2	42.0	0.0
402	4.47	6.5	25.2	32.4	332	4.69	29.8	49.3	44.7
420	4.47	6.6	25.6	0.0	005	5.00	28.5	23.3	31.3
422	4.90	161.9	141.2	140.9	403	5.00	28.7	55.3	60.5
224	4.90	161.9	142.5	147.1	510	5.10	28.2	19.7	20.0
333	5.20	110.5	91.7	97.7	314	5.10	28.3	49.7	47.6
511	5.20	110.5	97.1	98.2	423	5.39	27.2	12.6	0.0
115	5.20	110.4	98.4	96.4	205	5.39	27.3	74.3	71.5
					512	5.48	27.0	37.7	38.7

Class 3 reflections									
hkl	$\lvert G \rvert$	$\rho_{UR}(\mathbf{G})$	$\rho_R(\mathbf{G})$	$\rho_{expt}(\mathbf{G})$	*hkl*	$\lvert G \rvert$	$\rho_{UR}(\mathbf{G})$	$\rho_R(\mathbf{G})$	$\rho_{expt}(\mathbf{G})$
100	1.00	45.4	25.2	34.7	411	4.24	29.9	56.3	48.5
101	1.41	43.3	40.6	49.8	412	4.58	28.6	40.8	41.0
210	2.24	39.2	55.4	47.9	214	4.58	28.6	41.0	41.1
102	2.24	39.2	55.5	52.5	323	4.69	28.3	47.5	41.2
211	2.45	38.1	51.5	48.3	500	5.00	27.1	27.5	35.7
212	3.00	35.3	23.0	26.3	430	5.00	27.2	55.5	47.7
300	3.00	35.3	80.0	72.2	304	5.00	27.2	56.3	55.7
103	3.16	34.6	41.0	40.7	105	5.10	26.8	18.7	19.1
301	3.16	34.6	41.0	38.8	501	5.10	26.8	18.8	0.0
320	3.61	32.5	6.9	0.0	431	5.10	26.8	50.2	46.4
302	3.61	32.5	7.2	0.0	413	5.10	26.8	50.7	51.6
321	3.74	31.9	35.9	32.9	324	5.39	25.9	11.3	0.0
213	3.74	32.0	36.2	33.8	432	5.39	25.9	11.3	0.0
104	4.12	30.3	19.2	21.2	520	5.39	25.9	75.5	66.3
410	4.12	30.3	19.5	21.3	502	5.39	25.9	75.8	77.0
322	4.12	30.4	66.3	61.6	521	5.48	25.6	36.4	0.0
303	4.24	29.9	13.3	0.0	215	5.48	25.6	36.8	37.0

only the observed reflections presented in Table VI; higher values are obtained if the unobserved reflections [$\rho_{expt}(\mathbf{G})=0$] are included. The trend clearly indicates the superiority of the structural parameters determined by Kawano and Ueda to either the unrelaxed parameters or those determined via the pseudopotential total-energy calculation of De Pascale *et al.*[47]

VI. COMPARISON WITH EXPERIMENT

A. Photoemission

The states observed in $CdIn_2Se_4$ by x-ray photoemission[51] (XPS) and ultraviolet photoemission[50] (UPS) are summarized in Table VII, along with other experimental data for $CuInSe_2$,[62] CdSe,[63] and InSe.[64] Despite the lack of a density of states plot and the well-known[56] local-density eigenvalue error, a general identification of the main states appears possible.

The upper valence band of $CdIn_2Se_4$ (Fig. 7) consists of 12 bands; its top region (0.0 to 3 eV below the top of the valence band, E_v) was identified as the Se dangling-bond lone-pair band (Fig. 11). This portion, most likely, is responsible for the three structures (A, B, and B') observed in XPS. Since the vacancy dangling bond is "healed" effectively in this structure (it is not evident in the total charge density), we expect general similarities to the

TABLE VII. XPS and UPS observed binding energies (in eV, relative to the valence-band maximum) of some semiconducting selenides. UVB denotes the upper valence band.

Label[a]	$CdIn_2Se_4$ XPS[a]	$CdIn_2Se_4$ UPS[b]	Present interpretation	$CuInSe_2$[c]	CdSe[d]	InSe[e]
A	−0.9	−1.05	Upper lone-pair band	−0.5 to −3.2 UVB	−0.8 to −5.5 UVB	
B	−1.75	−1.75				
B'	−3.15					
B''	−4.45					
C	−5.9	−6.05	In–Se band (−4 to −6)	−6.2		
C'	−8.1		None			
Cd 4*d*	−10.0	−10.1	−9.5		−10.04	
Se 4*s*			−12.2	−13	−11.4	
In $4d_{5/2}$	−16.8		−16.0	−17		−17.3
In $4d_{3/2}$	−17.7					−18.3

[a]Margaritondo *et al.*, Ref. 51.
[b]Picco *et al.*, Ref. 50.
[c]Rife *et al.*, Ref. 62.
[d]Ley *et al.*, Ref. 63.
[e]Antonangeli *et al.*, Ref. 64.

upper valence region in other tetrahedral chalcogenides, e.g., $CuInSe_2$ and CdSe. This is generally supported by the data (Table VII).[62,63]

At higher binding energies, our calculation shows the In-Se band (Figs. 7 and 8) at E_v-4 to E_v-6 eV. This energy range is associated here with peak *C* at $E_v-5.9$ eV (Ref. 51) or $E_v-6.05$ eV.[50] A similar feature appears in $CuInSe_2$ (Ref. 62) at a similar energy of $E_v-6.2$ eV. This feature is unique to ternary systems, and is responsible for these systems having an upper valence band width which is ~0.5–1 eV larger than that of binary selenides. The shoulder (*C'*) at $E_v-8.1$ eV has no counterpart in our calculation and is also missing in the UPS spectra[50] and in the observed[62] and calculated[54] spectra of other chalcogenides. We are inclined to interpret this as a nonintrinsic (possibly, defect-related) structure.

The Cd 4*d* emission appears at E_v-10 eV and $E_v-10.04$ eV for $CdIn_2Se_4$ and CdSe, respectively, indicating similar ionicities in these materials. The calculated values ($E_v-9.5$ eV) for this state and the In 4*d* core state are 0.5–1.2 eV too shallow relative to experiment. This agreement with experiment is, in part, fortuitous: relativistic effects (neglected here) tend to move *d* states to *lower* binding energies[65] (since the contraction of the *s* electrons better screens the non-*s* electrons), while orbital relaxation effects attendant upon photoemission (neglected too) tend to *increase* the binding energy[66] (the latter effect is overwhelming in low-*Z* materials).

Note that the In 4*d* peak in InSe (Ref. 64) appears at higher binding energies relative to $CdIn_2Se_4$, suggesting a larger covalency in the latter case.

Margaritondo *et al.*[51] suggest that the Se 4*s* states are missing from their spectra because of low photoionization cross section at the photon energies they used. The Baldereschi *et al.*[23] calculation places these states at about −15 eV, nearly 3 eV deeper than our calculation, for reasons discussed in Sec. V B.

B. Absorption and photoconductivity

Because of the probable existence of multiple phases in currently prepared $CdIn_2Se_4$ crystals (see Sec. III B) it is difficult to interpret the optical spectra in any simple way. Koval *et al.*[37] measured absorption of single crystals grown by chemical transport. They observed optical transitions at 1.51 eV and 1.73 eV. The absorption coefficient α was calculated from the optical transmission and reflection spectra with multiple reflections taken into account. They determined the nature of the observed transitions by plotting $\alpha^{1/2}$ and α^2 as a function of photon energy. Simple models[67] indicate that for indirect transitions $\alpha^{1/2}$ should approach a straight line far enough (but not too far) above the absorption edge, and for direct transitions α^2 should do the same. As a result Koval *et al.* concluded that the transition at 1.51 eV was indirect, and that at 1.73 eV was direct. Their published plots show only $\alpha^{1/2}$ for the transition believed to be indirect, and α^2 for the transition believed to be direct. The relative intensities of the two transitions are consistent with what would be expected if their interpretation is correct. Note, however,[67] that in most cases for direct transitions the observed behavior is that α is more closely proportional to the 3/2 rather than the 1/2 power of the excess photon energy. The 1/2 power is expected for allowed direct transitions, whereas the 3/2 power is expected for forbidden direct transitions. Surprisingly, the data of Koval *et al.*[37] appear to be an ex-

ception to this usual behavior.[67]

Koval *et al.*[37] also measured reflectivity of the material, and found peaks at 1.95, 2.50, 3.55, and 4.15 eV, all attributed to higher direct transitions. Trykozko[34,68] did photoconductivity, absorption, and thermoreflectance measurements at room temperature and at liquid-nitrogen temperature on samples prepared by chemical transport. For the photoconductivity measurements, the distinction between the direct and indirect transitions was made on the following basis. When a small area of the sample was illuminated near the center of the sample (away from the electrodes), the spectral peak at lower energy (about 1.5 to 1.6 eV) was higher than the higher-energy peak (about 1.9 eV), whereas, when an area near one of the electrodes was illuminated, the higher-energy peak had the greater height. The explanation offered was that the direct absorption is stronger, hence penetration into the sample was smaller in that case, and surface recombination reduced the collected current when the illuminated area was far from the electrodes. In contrast, the indirect absorption, being weaker, allowed greater penetration, reducing the relative importance of surface recombination in that energy range. Of course, any transition which is weaker than the direct transition would show similar behavior, so the argument is not conclusive. The values of the energy gaps were determined via Moss criteria. Fortin and Raga[69] have observed a photoconductivity peak at 1.57 eV, *lower* than the reflectivity peak at 2.0 eV. They suggest the lower energy state to be the true minimum gap of the system and that it corresponds to an *indirect* gap. However, Mekhtiev and Guseinov[70] have identified the luminescence peaks at 1.29–1.59 eV as impurity acceptor states and placed the true band gap (direct or indirect) at 1.90 eV at 2 K.

There is evidence accumulating[37,71] that the observed band gap of the β modification of $CdIn_2Se_4$ [Fig. 1(g)] is a result of band tailing of the conduction band as a consequence of disorder, resulting in a smaller gap (~ 1.30 eV) than in the pseudocubic α form. Consideration of this information may be relevant because of the very similar environments of the atoms in the α and β structures. Indeed the observed band gaps of the two are only slightly different.[72] Fortin and Raga[69] present absorption and photoconductivity data for β-$CdIn_2Se_4$, noting the absence of evidence of excitons. Their hypothesis on the reason for this is that excitons are very sensitive to lattice defects, and that the vacant nature of the structure may give rise to a large number of defects which would be difficult to see in x-ray spectra. Georgobiani *et al.*[73] have studied the temperature dependence of the absorption edge in β-$CdIn_2Se_4$ and concluded that there is a quasicontinuous distribution of states in a tail below the bottom of the conduction band, most probably caused by disorder. Annealing and rapid quenching of the samples reduced the band gap further (about 40–50 meV), whereas annealing followed by slow cooling had little effect. Mekhtiev *et al.*[74] reported that thermally stimulated current and space-charge-limited current studies showed electron trapping levels with an exponential distribution in the energy interval from 0.1 to 0.21 eV from the bottom of the conduction band in β-$CdIn_2Se_4$. As a consequence of these results and the results of our calculation, we feel that it is as yet too early to draw final conclusions on the nature of the band gap in α-$CdIn_2Se_4$.

VII. SUMMARY AND CONCLUSIONS

Referring to the questions raised in Sec. II D concerning the electronic structure of $CdIn_2Se_4$, we conclude the following.

(i) The OVC $CdIn_2Se_4$ is characterized by a spectral range of the topmost ~ 3 eV of the valence band in which lone-pair Se dangling orbitals exist. They span a variety of orientations relative to the neighboring anions (Fig. 11), show up in photoemission (Table VII) and control the low-energy interband optical transitions.

(ii) These dangling-bond-like states, analogous to those in cation vacancies in II-VI compounds broaden into a band, filling up the gap between them; no valence-band gap is hence evident (in agreement with the photoemission data). These states contain both anion-localized and nearly overlapping members (Fig. 11).

(iii) The $CdIn_2Se_4$ structure is characterized by an anion displacement, relative to the zinc-blende configuration. The anion moves toward the vacancy (and away from the Cd and In sites) by about 0.1 Å. This displacement reflects predominantly the need to accomodate the dissimilar In—Se and Cd—Se bonds in the same unit cell and hence manifests the tendency of these covalent bonds to attain their ideal tetrahedral lengths (Table II), at the expense of small distortions in the bond angles (Fig. 4). A conservation of tetrahedral bonds model accounts well for the observed displacements (Fig. 4).

(iv) A characteristic feature of $CdIn_2Se_4$ relative to binary covalent semiconductors (CdSe and InSe) is the appearance of a distinct In-Se band at the bottom of the upper valence band, in addition to the In-Se+Cd-Se bands above it. This In-Se band increases the width of the upper valence band relative to the binary systems by ~ 1 eV and appears in the XPS spectrum.

In addition to these issues, we have noted the following.

(a) The small difference between the valences of the two cations (two and three, for Cd and In, respectively), combined with the existence of a sublattice of vacant sites, makes this class of materials susceptible to a few possible order-disorder transitions whereby the cations substitute on the same sublattice or also on the vacancy sublattice. This degree of disorder as well as the existence of phases other than the α form in currently grown $CdIn_2Se_4$ crystals makes the interpretation of the optical data difficult. We find a direct gap, whereas most experimental studies suggest an indirect gap. The latter could, however, represent transitions associated with disorder or with multiple-phase coexistence.

(b) The band structure of $CdIn_2Se_4$ lends itself to partitioning into five major subbands in the 0 to -16 eV region. These are (i) the lone-pair upper band (0 to ~ -4.5 eV) containing mostly Se p, with smaller amounts of In s and p, and Cd s and Cd p character, (ii) the In s–Se p band (-4 to -6 eV), (iii) the Cd $4d$ band (-9.5 eV), (iv) the Se $4s$ band, showing also Cd $4d$ char-

acter (−12.5 eV), and (v) the In 4*d* band (−16 eV). Each of these subbands is characterized by distinct features in the bonding pattern, evidenced in band-by-band charge density plots (Fig. 8) and in the XPS spectra (Table VII). Previous calculations, using either empirical[23,46] or self-consistent[47] pseudopotentials lacking Cd *d* states exhibit systematic deviations from the present all-electron study.

(c) Relaxation of the "ideal" structure has only subtle effects on the band structure, leaving the band gap unchanged and reducing the width of the upper valence band by 0.6 eV (a bonding state, destabilized by an increase in the Cd—Se and In—Se bond lengths upon relaxation).

(d) The total valence charge density shows a nearly complete "repair" of the vacant site, with little charge density there. The Fourier transform of the charge density (x-ray scattering factors) was analyzed in terms of sublattices, aiding the possibility of assessing the degree of order or disorder by comparing calculated to measured scattering factors.

ACKNOWLEDGMENTS

We wish to thank S. Kawano for kindly providing us with additional information regarding the structural determination of pseudocubic $CdIn_2Se_4$ reported in Ref. 35. This work was supported by the Office of Energy Research, Materials Science Division, U.S. Department of Energy, under Grant No. DE-AC02-77-CH00178.

[1]E. Parthé, *Crystal Chemistry of Tetrahedral Structures* (Gordon and Breach, New York, 1964), pp. 149, 152.

[2]N. A. Goryunova, *The Chemistry of Diamond-Like Semiconductors* (MIT Press, Cambridge, 1965), p. 152.

[3]L. Shay and J. H. Wernick, *Ternary Chalcopyrite Semiconductors: Growth, Electronic Properties and Applications* (Pergamon, Oxford, 1974).

[4]U. Kaufmann and J. Schneider, in *Festkorperprobleme* (Vieweg, Braunschweig, 1974), Vol. XIV, p. 229.

[5]S. Wagner, in *Electroluminescence,* edited by J. I. Pankove (Springer, Berlin, 1977), p. 171.

[6]A. MacKinnon, in *Festkorperprobleme,* edited by J. Treusch (Vieweg, Dortmund, 1981), Vol. XXI, p. 149.

[7]A. Miller, A. MacKinnon, and D. Weaire, in *Solid State Physics,* edited by H. Ehrenreich, F. Seitz, and D. Turnbull (Academic, New York, 1981), Vol. 36, p. 119.

[8]*Deuxieme Conference Internationale sur les Composes Semiconducteurs Ternaires, Strasbourg, 1975* [J. Phys. (Paris) Colloq. **36** (C-3) (1975)].

[9]*Ternary Compounds, 1977, Proceedings of the Edinburgh Conference on Ternary Compounds,* Inst. Phys. Conf. Ser., Vol. 35, edited by G. D. Holah (Institute of Physics, Bristol and London, 1977).

[10]*Proceedings of the Fourth International Conference on Ternary and Multinary Compounds, Tokyo, Japan, 1980* [Jpn. J. Appl. Phys. **19** (Suppl. 19-3) (1980)].

[11]*Proceedings of the Fifth International Conference on Ternary and Multinary Compounds, Cagliari, Italy, 1982* [Nuovo Cimento D **2** (6) (1983)].

[12]*Proceedings of the Sixth International Conference on Ternary and Multinary Compounds, Caracas, Venezuela, 1984,* edited by B. R. Pamplin, N. V. Joshi, and C. Schwab [Prog. Crystal Growth Characterization **10** (1984)].

[13]*Ternary and Multinary Compounds: Proceedings of the Seventh International Conference, Snowmass, Colorado, September 10-12, 1986,* edited by S. K. Deb and A. Zunger (Materials Research Society, Pittsburgh, Pennsylvania, 1987).

[14]T. S. Kuan, T. F. Kuech, W. I. Wang, and E. L. Wilkie, Phys. Rev. Lett. **54**, 201 (1985).

[15]C. B. Sclar and M. Drovenik, Bull. Geolog. Soc. Am. **71**, 1970 (1960), describe the structure of lazarevicite; a mineral with the same structure, $Cu_3(As,V)S_4$, called *arsenosulvanite* was described by A. G. Betekhtin, Zapiski Vses. Mineral. Obshch. (Mem. Soc. Russe Mineral) **70**, 161 (1941), and V. I. Mikheev, *ibid.*, **70**, 165 (1941).

[16]The famatinite form was recently observed for $InGa_3As_4$ and In_3GaAs_4; see H. Nakajama and H. Fujita, in *GaAs and Related Compounds 1985,* Inst. Phys. Conf. Ser., Vol. 79, edited by M. Fujimoto (Hilger, Bristol, 1986), p. 289.

[17]A. N. Georgobiani, S. I. Radautsan, and I. M. Tiginyanu, Fiz. Tekh. Poluprovodn. **19**, 193 (1985) [Sov. Phys.—Semicond. **19**, 121 (1985)]; C. Razzetti, P. P. Lottici, and L. Zanotti, Mater. Chem. Phys. **11**, 65 (1984).

[18]A. MacKinnon, in *Landolt-Bornstein, Numerical Data and Functional Relationships in Science and Technology, New Series, Group III* (Springer, Berlin, 1985), Vol. 17h, p. 124.

[19]A. F. Wells, *Structural Inorganic Chemistry,* 4th ed. (Clarendon, Oxford, 1975), p. 570, discusses lone pairs around S, Se, and Te containing molecules.

[20]I. C. Bowater, R. D. Brown, and F. R. Burden, J. Mol. Spectrosc. **28**, 461 (1968).

[21]G. D. Watkins, in *Radiation Effects in Semiconductors* (Gordon and Breach, London, 1971), p. 301; K. M. Lee and G. D. Watkins, in *Proceedings of the Conference on Defects in Semiconductors, Kyoto, 1980,* Inst. Phys. Conf. Ser., Vol. 59 (Institute of Physics, London, 1981), p. 353.

[22]M. Jaros, J. Cryst. Growth **72**, 139 (1985); P. Pecheur, J. Van der Rest, and G. Toussaint, *ibid.* **72**, 147 (1985); P. H. E. Meijer, P. Pecheur, and G. Toussaint, Phys. Status Solidi B **140**, 155 (1987).

[23]A. Baldereschi, F. Meloni, F. Aymerich, and G. Mula, Solid State Commun. **21**, 113 (1977).

[24]D. J. Stuckel, R. N. Euwema, T. C. Collins, F. Herman, and R. L. Kortum, Phys. Rev. **179**, 740 (1969); T. K. Bergstresser and M. L. Cohen, *ibid.* **164**, 1069 (1967).

[25]V. K. Bazhenov, D. I. Marvakov, and A. G. Petukhov, Fiz. Tekh. Poluprovodn. **13**, 1482 (1979) [Sov. Phys.—Semicond. **13**, 866 (1979)]; Y. Depeursinge, E. Doni, R. Girlanda, A. Baldereschi and K. Maschke, Solid State Commun. **27**, 1449 (1978); A. Bourdon, A. Chevy and J. M. Besson, in *Physics of Semiconductors 1978,* Inst. Phys. Conf. Ser., Vol. 43, edited by B. L. H. Wilson (Institute of Physics, Bristol, 1978), p. 1371.

[26]C. Froese-Fischer, *The Hartree-Fock Method for Atoms* (Wiley, New York, 1977).

[27]H. Hahn, G. Frank, W. Klingler, A.-D. Storger, and G. Storger, Z. Anorg. Allg. Chem. **279**, 241 (1955).

[28]G. F. Mocharnyuk, T. I. Babyuk, O. P. Derid, L. S. Lazarenko, M. M. Markus, and S. I. Radautsan, Dokl. Akad. Nauk

SSSR **237**, 821 (1977) [Sov. Phys.—Dokl. **22**, 749 (1977)].
[29]B. E. Mellander and M. Friesel, Phys. Rev. B **35**, 7902 (1987).
[30]A. Zunger, Appl. Phys. Lett. **50**, 164 (1987).
[31]M. A. Ryan, M. W. Peterson, D. L. Williamson, J. S. Frey, G. E. Maciel, and B. A. Parkinson, J. Mater. Res. **2**, 528 (1987).
[32]C. Rincon and S. M. Wasim, in *Ternary and Multinary Compounds: Proceedings of the Seventh International Conference, Snowmass, Colorado, September 10-12, 1986,* edited by S. K. Deb and A. Zunger (Materials Research Society, Pittsburgh, Pennsylvania, 1987), p. 413; D. Cahen, *ibid.*, p. 433.
[33]P. Kistaiah, K. Satyanarayana Murthy, and K. V. Krishna Rao, Phys. Status Solidi B **71**, K225 (1982).
[34]R. Trykozko, in *Ternary Compounds, 1977, Proceedings of the Edinburgh Conference on Ternary Compounds,* Inst. Phys. Conf. Ser., Vol. 35, edited by G. D. Holah (Institute of Physics, Bristol and London, 1977), p. 249.
[35]S. Kawano and I. Ueda, Mem. Fac. Sci., Kyushu Univ., Ser. B **3** (5), 127 (1967).
[36]H. Suzuki and S. Mori, J. Phys. Soc. Jpn. **19**, 1082 (1964).
[37]L. S. Koval, M. M. Markus, S. I. Radautsan, V. V. Sobolev, and A. V. Stanchu, Phys. Status Solidi A **9**, K69 (1972).
[38]J. Przedmojski and B. Palosz, Phys. Status Solidi A **51**, K1 (1979).
[39]C. Manolikas, D. Bartzokas, G. vanTendeloo, J. vanLanduyt, and S. Amelinckx, Phys. Status Solidi A **59**, 425 (1980).
[40]J. E. Jaffe and A. Zunger, Phys. Rev. B **29**, 1882 (1984).
[41]L. Pauling, *The Nature of the Chemical Bond,* 3rd ed. (Cornell University, Ithaca, 1960), p. 246. The CTB construct of Eq. (4) cannot be used in structures with different site symmetries for the same chemical species. In these there can be more than one type of bond for a given pair of atoms, and the concept of unique atomic radii breaks down. An example is the defect-chalcopyrite ($I\bar{4}$) structure of Fig. 1(g), characterized by *three cell-internal parameters (x,y,z) and two distinct B—C bonds in* AB_2C_4. Hence, the In—Se bond lengths (Ref. 27) in $HgIn_2Se_4$ (2.60 Å and 2.56 Å) or in $ZnIn_2Se_4$ (2.44 Å and 2.57 Å) differ from the CTB ideal value of 2.58 Å. In the undistorted $I\bar{4}$ structure ($x=y=1/4$; $z=1/8$), the two B—C bond lengths are equal, and the CTB model can be expected to work.
[42]A. D. Stuckes and G. Farrell, J. Phys. Chem. Solids **25**, 477 (1964).
[43]H. W. Spiess, V. Haeberlen, G. Brandt, A. Rauber, and J. Schneider, Phys. Status Solidi B **62**, 183 (1974).
[44]J. E. Jaffe and A. Zunger, Phys. Rev. B **30**, 741 (1984).
[45]See, e.g., J. L. Martins and A. Zunger, Phys. Rev. B **32**, 2689 (1985).
[46]A. Baldereschi and F. Meloni, in *Proceedings of the 4th International Conference on Ternary and Multinary Compounds, Tokyo, 1980* [Jpn. J. Appl. Phys. **19** (Suppl. 19-3), 161 (1980)].
[47]T. M. De Pascale, M. Marinelli, F. Meloni, G. Mula, M. Serra, and P. Giannozzi, in *Ternary and Multinary Compounds: Proceedings of the Seventh International Conference, Snowmass, Colorado, September 10-12, 1986,* edited by S. K. Deb and A. Zunger (Materials Research Society, Pittsburgh, Pennsylvania, 1987).
[48]K. C. Hass and D. Vanderbilt, in *18th International Conference on the Physics of Semiconductors,* edited by O. Engstrom (World Scientific, Singapore, 1987), p. 1181; see also K. J. Chang, S. Froyen, and M. L. Cohen, Phys. Rev. B **28**, 4736 (1983).
[49]S.-H. Wei and A. Zunger, Phys. Rev. Lett. **59**, 144 (1987).
[50]P. Picco, I. Abbati, L. Braicovich, F. Cerrina, F. Levy, and G. Margaritondo, Phys. Lett. **65A**, 447 (1978).
[51]G. Margaritondo, A. D. Katani, and F. Levy, Phys. Status Solidi B **103**, 725 (1981).
[52]V. I. Chizhikov, V. L. Panyutin, B. E. Ponedelnikov, and A. E. Rozenson, J. Phys. (Paris) **42**, 1039 (1981).
[53]F. Cerrina, C. Quaresima, I. Abbati, L. Braicovich, P. Picco, and G. Margaritondo, Solid State Commun. **33**, 429 (1980).
[54]P. Bendt and A. Zunger, Phys. Rev. B **26**, 3114 (1982).
[55]D. M. Ceperley and B. J. Alder, Phys. Rev. Lett. **45**, 566 (1980).
[56]J. P. Perdew and Alex Zunger, Phys. Rev. B **23**, 5048 (1981).
[57]A. I. Gubanov and F. M. Gashimzade, Fiz. Tverd. Tela (Leningrad) **1**, 1411 (1959) [Sov. Phys.—Solid State **1**, 1294 (1960)].
[58](a) F. Aymerich, F. Meloni, and G. Mula, Phys. Rev. B **15**, 3980 (1977); (b) F. Aymerich, A. Baldereschi, F. Meloni, and G. Mula, in *Physics of Semiconductors: Proceedings of the 13th International Conference,* edited by F. G. Fumi (North-Holland, Amsterdam, 1976), p. 154; (c) F. Aymerich, G. Mula, A. Baldereschi, and F. Meloni, in Ref. 9, p. 159.
[59]*International Tables for X-Ray Crystallography* (Kynoch, Birmingham, England, 1962), Vol. III, pp. 210–212.
[60]J. L. Martins and A. Zunger, J. Mater. Res. **1**, 523 (1986).
[61]J. E. Bernard and A. Zunger, Phys. Rev. B **36**, 3199 (1987).
[62]J. Rife, R. N. Dexter, P. M. Bridenbaugh, and B. W. Veal, Phys. Rev. B **16**, 4491 (1977).
[63]L. Ley, R. A. Pollak, F. R. McFeely, S. P. Kowalczyk, and D. A. Shirley, Phys. Rev. B **9**, 600 (1974); N. J. Shevchik, J. Tejeda, M. Cardona, and D. W. Langer, Phys. Status Solidi B **59**, 87 (1973).
[64]F. Antonangeli, M. Piacentini, A. Balzarotti, V. Grasso, R. Girlanda, and E. Dons, Nuovo Cimento B **51**, 181 (1979).
[65]S.-H. Wei, A. A. Mbaye, L. G. Ferreira, and A. Zunger, Phys. Rev. B **36**, 4163 (1987).
[66]A. Zunger and A. J. Freeman, Phys. Rev. B **16**, 2901 (1977).
[67]R. A. Smith, *Semiconductors,* 2nd ed. (Cambridge University, Cambridge, 1978), p. 309.
[68]R. Trykozko and D. R. Huffman, J. Appl. Phys. **52**, 5283 (1981).
[69]E. Fortin and F. Raga, Solid State Commun. **14**, 847 (1974).
[70]N. M. Mekhtiev and Z. Z. Guseinov, Fiz. Tekh. Poluprovodn. **20**, 2103 (1986) [Sov. Phys.—Semicond. **20**, 1313 (1986)].
[71]V. V. Sobolev, Izv. Akad. Nauk Mold. SSR, Ser. Fiz.-Tekh. Mat. Nauk, No. 2, 60 (1976); Izv. Akad. Nauk SSSR, Neory Mat **8**, 26 (1972).
[72]T. G. Kerimova, F. R. Adyalova, A. Sh. Khidirov, and E. Yu. Salaev, Phys. Status Solidi A **71**, K211 (1982).
[73]A. N. Georgobiani, I. M. Tiginyanu, and V. V. Ursaki, Fiz. Tekh. Poluprovodn. **20**, 1914 (1986) [Sov. Phys.—Semicond. **20**, 1201 (1986)].
[74]N. M. Mekhtiev, Z. Z. Guseinov, and E. Yu. Salaev, Fiz. Tekh. Poluprovodn. **19**, 1642 (1985) [Sov. Phys.—Semicond. **19**, 1010 (1985)].

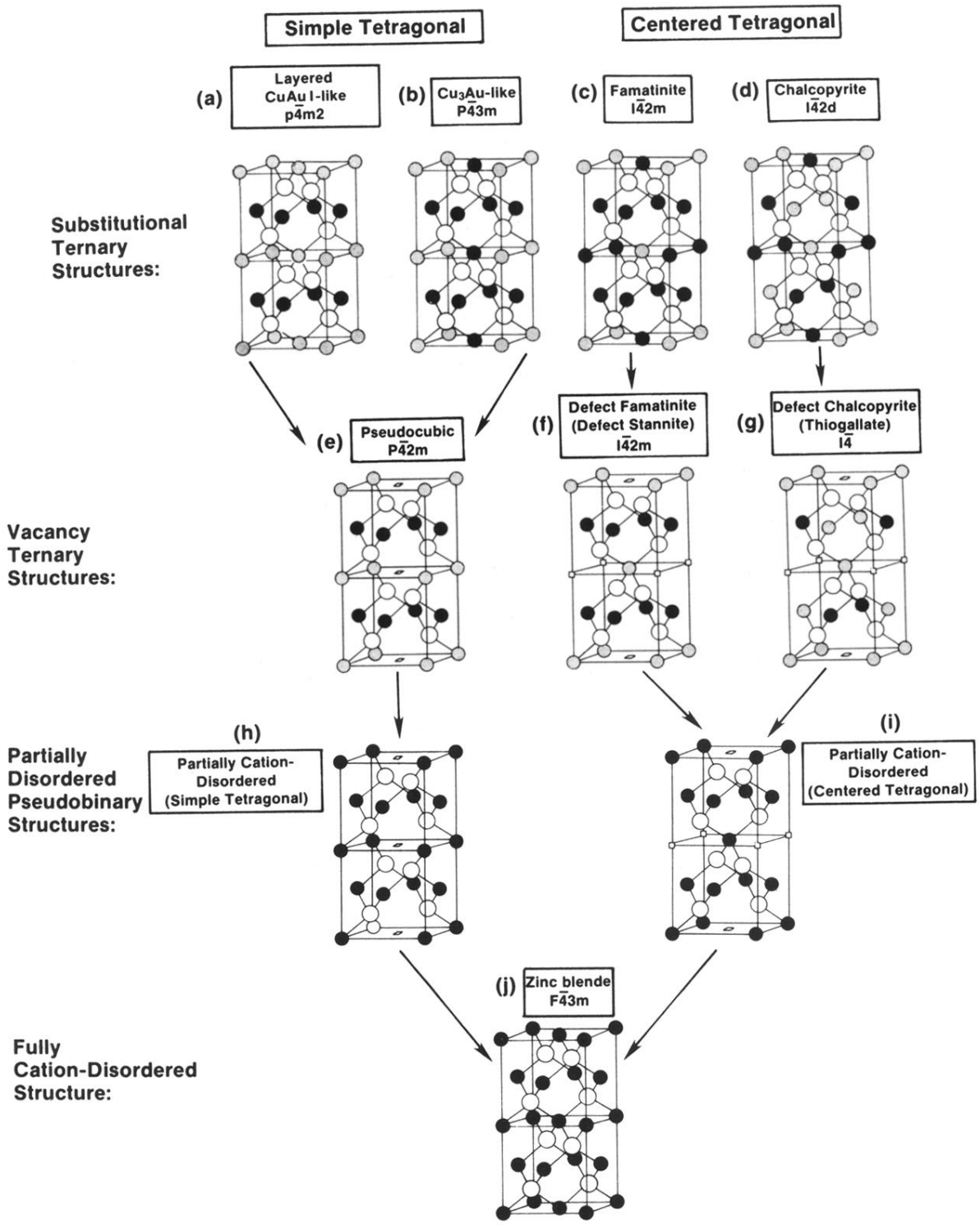

FIG. 1. Crystal structure of ternary $A_nB_{4-n}C_4$ adamantine compounds (a)–(d), vacancy structures derived from them (e)–(g), and two stages of cation disorder of the vacancy structures: Stage I, (h) and (i); and stage II, (j).

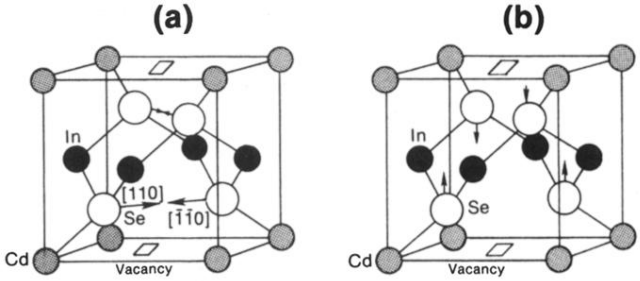

FIG. 3. Space-group preserving internal relaxations possible in the structure of pseudocubic $CdIn_2Se_4$. (a) shows the displacement of the anions as the parameter x is increased, and (b) shows the displacement as the parameter z is increased. See Eqs. (1) and (2). A square denotes the vacant site.

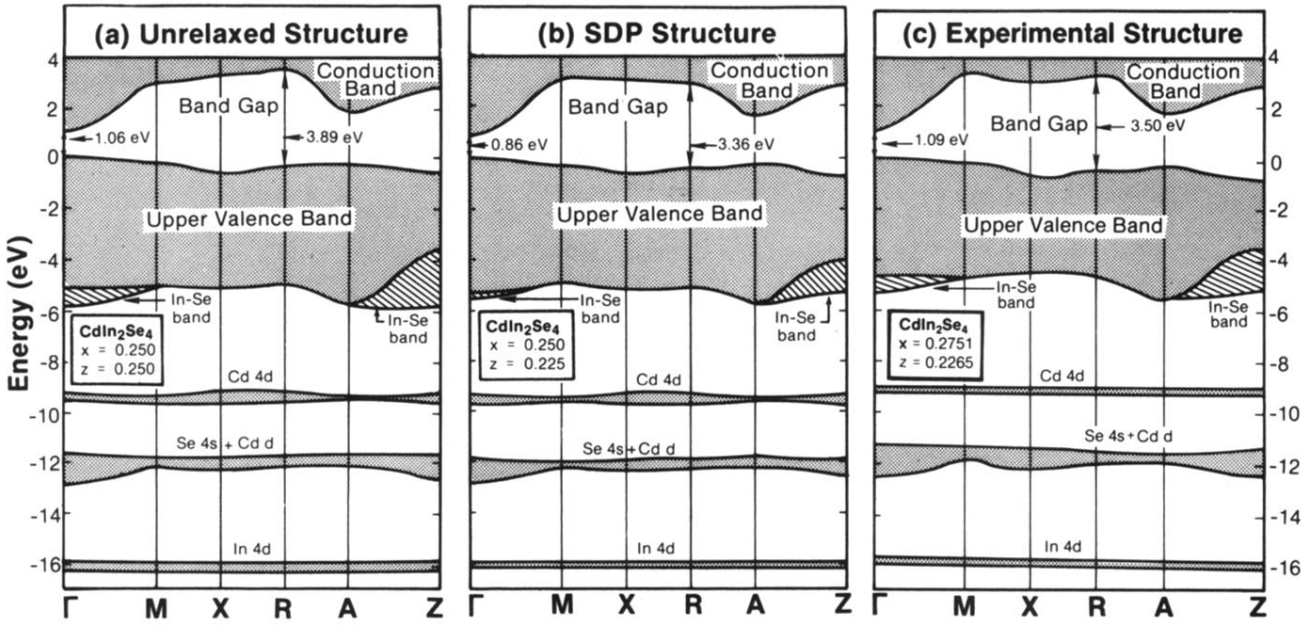

FIG. 7. Band structures calculated at six high-symmetry points for (a) the unrelaxed structure, (b) the scaled De Pascale structure, and (c) the experimental structure. All were calculated at a lattice constant of $a = 5.815$ Å. Rather than show the complex bands within each subband, we delineate the regions of the main groups of bands.

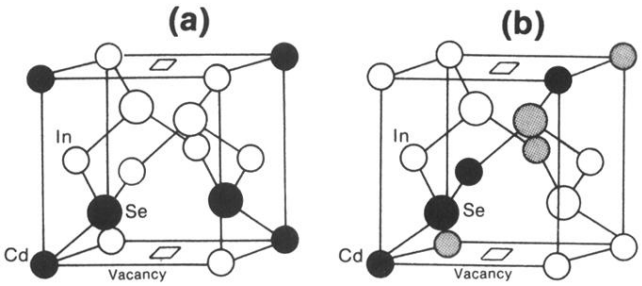

FIG. 9. Plot planes used for charge density plots. (a) shows the *vacancy* plane, which includes the solid atoms and the vacancies, and (b) shows the *indium* plane, the solid atoms being in the plane for all values of the structural parameters x and z, and the grey atoms being in the plane only for the unrelaxed values of the parameters.